Geochemistry, Geophysics, Geosystems®

AGU ADVANCING EARTH AND SPACE SCIENCE

RESEARCH ARTICLE
10.1029/2022GC010566

Special Section:
Frontiers in lithospheric dynamics: bridging scales through observations, experiments, and computations

Insights on Formation of the Gulf of Mexico by Rayleigh Surface Wave Imaging

Luan C. Nguyen[1], Alan Levander[1], Fenglin Niu[1], Julia Morgan[1], and Guoliang Li[2]

[1]Department of Earth, Environmental and Planetary Sciences, Rice University, Houston, TX, USA, [2]Southern California Earthquake Center, University of Southern California, Los Angeles, CA, USA

Key Points:

- Inherited lithospheric thickness controls spatial and temporal rate of rifting
- Refertilization of the mantle lithosphere drives development of mantle shear-zones
- Deformable plate modeling shows extension toward the southeast during the Mesozoic rifting of the Gulf of Mexico continental margins

Supporting Information:

Supporting Information may be found in the online version of this article.

Correspondence to:

L. C. Nguyen,
luan.c.nguyen@rice.edu

Citation:

Nguyen, L. C., Levander, A., Niu, F., Morgan, J., & Li, G. (2022). Insights on formation of the Gulf of Mexico by Rayleigh surface wave imaging. *Geochemistry, Geophysics, Geosystems*, *23*, e2022GC010566. https://doi.org/10.1029/2022GC010566

Received 7 JUN 2022
Accepted 17 NOV 2022

Abstract We used cross-correlation of ambient noise records from seismic stations in the US, Mexico, and Cuba to extract dispersion data of Rayleigh surface wave. Our derived 3D shear-wave velocity model of the greater Gulf of Mexico (GOM) region captures variations in the crustal and lithospheric structures across the continental margins of the US Gulf Coast and Yucatan, Mexico. The model shows a zone of reduced velocity in the mantle lithosphere underlying the extended continental margin of the northwestern GOM. We attributed this velocity reduction to extensional deformation and melt-induced weakening of the lithosphere during the Triassic continental rifting that preceded the seafloor spreading that formed the GOM. Melt extraction might have been hindered by the greater lithospheric thickness in the western region along the US Gulf Coast margin that resulted in the westward decrease of rift-related volcanism/magmatism reported from previous studies. The clear asymmetry between the US Gulf Coast and its conjugate Yucatan margin suggests extension along a shear-zone that focused more deformation on the North American plate prior to breakup. In contrast to the counterclockwise rotation of the Yucatan block during seafloor-spreading, our analyses using deformable plate models demonstrate that continental rifting occurred in a predominantly northwest-southeast direction. This change in plate motion is attributed to the development of mantle shear-zones in the western part of the rift. We estimated the depth of the lithosphere-asthenosphere boundary and determined that the extended continental and oceanic lithospheres have mostly regained their thickness since the time of breakup.

1. Introduction

1.1. Geographic Setting

Passive margins mark the region where the lithospheric plates break apart and the transition from continental to an oceanic domain takes place. This geologic region preserves a record of the tectonic, magmatic, and sedimentary processes that accompany continental extension and therefore is important to the understanding of plate tectonics. In this study, we investigated the margins surrounding the Gulf of Mexico (GOM), as well as the deep GOM ocean itself, to better understand the Triassic-Jurassic breakup of the North and South American plates during the opening of the Atlantic. The GOM is a relatively small ocean basin situated south of the continental US that is surrounded on the east, north, and west by the North American plate, and on the south by Cuba. The GOM is connected to the Atlantic Ocean through the Florida Straits and to the Caribbean Sea through the Yucatan Channel (Figure 1). A large part of the GOM is occupied by continental margins made up of stretched continental lithosphere with a small ocean basin in the center. The US Gulf Coast margin and the margin offshore Yucatan formed as a conjugate pair during a period of rifting beginning in Late Triassic (~200 Ma) followed by seafloor spreading starting and ceasing between ~160 and ~140 Ma (Hudec et al., 2013; Marton & Buffler, 1994; Pindell, 1985; Sawyer et al., 1991). In general, the GOM basin opened as the Yucatan block (YB) together with the South American plate separated from the North American plate.

1.2. Previous Studies

A significant number of geophysical studies in the offshore GOM region began more than six decades ago with marine seismic refraction and reflection surveys mapping thin continental and oceanic crusts at various locations throughout the GOM (Ebeniro et al., 1986, 1988; Ewing et al., 1960; Ibrahim & Uchupi, 1982; Ibrahim et al., 1981; Ladd et al., 1976; Nakamura et al., 1988). In this early phase of exploration, the direction of basin opening was not well constrained due to the lack of coherent seafloor-spreading magnetic isochrons, signals from which are greatly subdued by the thick sedimentary layer overlying the GOM basement. The distribution

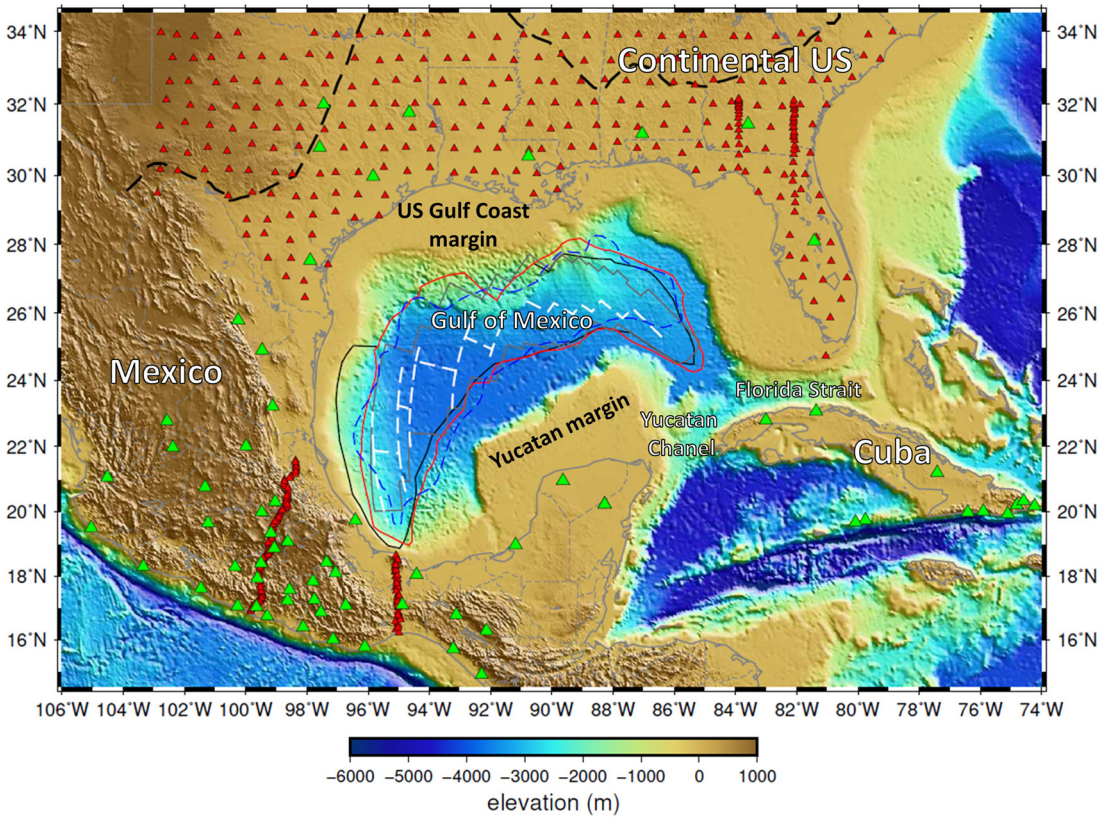

Figure 1. Geographic setting of the Gulf of Mexico (GOM) showing locations of all seismograph stations (triangles) used in this study. Temporary and permanent stations are showed in red and green, respectively. The white dashed lines are extinct spreading system active during the Jurassic opening of the GOM (Nguyen & Mann, 2016). The black dashed line traces the Ouachita, Appalachian mountain ranges. The colored outlines in the central basin marks distribution of oceanic crust from previous studies: red (Hudec et al., 2013), gray (Minguez et al., 2020), and black (Izquierdo-Llavall et al., 2022). Limit of crystalline crust with thickness <10 km derived from this study is shown with the blue dashed outline.

of oceanic crust was also poorly constrained as seismic mapping of the GOM's crustal structure covered only a small part of the basin. Early plate reconstruction models for the opening of the GOM were mostly based on regional plate kinematics drawn from the opening of the Atlantic (Klitgord et al., 1984; Pindell, 1985; Pindell & Dewey, 1982). As more data became available, understanding of the YB's paleo-motion evolved with analyses of marine gravity (Hall et al., 1982) and magnetic data (Hall & Najmuddin, 1994). Nevertheless, these studies yielded contradicting results with one suggesting a clockwise rotation of the YB while the other indicating a counterclockwise motion. Several workers have attempted a full-fit plate reconstruction to restore the YB to its pre-rift configuration. Dunbar and Sawyer (1987) estimated crustal thickness from tectonic subsidence analysis and restored the YB using a single pole of rotation for both periods of continental extension and seafloor spreading. In contrast, the kinematic model of Marton and Buffler (1994) restored the YB in a northwest-southeast (NW-SE) direction during extension, implying a different pole from that during seafloor spreading. Part of the puzzle of how the GOM opened was subsequently resolved with the release of satellite-derived gravity data (Sandwell et al., 2014) which provided the needed constraints on plate motion during the period of seafloor spreading. The geometry of the extinct spreading system consisting of ridges, and fracture zones, highlighted from gravity data confirmed the counterclockwise motion of the YB as it drifted away from the North American plate in the late Jurassic time (García-Reyes & Dyment, 2022; Minguez et al., 2020; Nguyen & Mann, 2016). Recent research has focused on the rifted margins surrounding the ocean basin to gain insight into the transitional process between the end of rifting and the initiation of seafloor spreading (Agrawal et al., 2015; Ainsworth et al., 2014; Evanzia et al., 2014). While interpretation of modeling of potential field data suggested a volcanic rifted margin along the Texas Gulf Coast (Mickus et al., 2009), the GUMBO wide-angle seismic refraction program along the northern GOM margin has shown the western US Gulf Coast margin as magma poor with little evidence of volcanic emplacement and/or magmatic intrusion (Van Avendonk et al., 2015). In addition, this

margin becomes progressively more volcanic eastward where seaward dipping reflectors and crustal underplating are both well imaged (Christeson et al., 2014; Eddy et al., 2014, 2018). In addition, presence of exhumed serpentinized mantle along the northern GOM margin has been proposed from analysis of aeromagnetic data (Minguez et al., 2020; Pindell et al., 2016). More modern seismic reflection profiles also suggest segments of exhumed mantle as well as magmatic intrusion/extrusion along the Yucatan margins (Izquierdo-Llavall et al., 2022). These findings together show strong variation in crustal structures along the rifted margins surrounding the GOM that could hold key insights to the processes of continental breakup. Although great progress has been made in the overall understanding of the opening history of the GOM, detail kinematics and geodynamics regarding the lithospheric evolution during basin formation remain to be fully revealed (Filina et al., 2022).

1.3. Study Objectives

At the current state, seismic studies in the GOM have provided great details in the structures and physical properties of the subsurface, but data are generally limited to localized areas within the northern GOM margin, with few studies focusing on the Yucatan margin (Filina & Hartford, 2021; Izquierdo-Llavall et al., 2022). Modeling of gravity and magnetic anomalies has provided improved spatial coverage of the GOM but lacks depth resolution. In addition, most studies have mainly focused on crustal structure even though continental extension and breakup involve the entire lithosphere, that is, both the crust and upper mantle. In this study, we constrained the crustal and lithospheric structures of the GOM region with a new 3D shear-wave velocity model. In addition to improving regional understanding of the GOM tectonic history, this broadens knowledge of the evolution of the continental lithosphere through periods of continental rifting and ensuing seafloor spreading as well as the development of oceanic lithosphere. Furthermore, recent studies that probe deeper beyond the crust in the western part of the US Gulf Coast margin have indicated presence of a thermal anomaly in the upper mantle (Krauss & Menke, 2020; Yao & Li, 2016). The hypothesis that the GOM opened due to a mantle plume impact had been proposed by Bird et al. (2005). Using our velocity model, we examined whether any signature of a thermal anomaly in the asthenosphere could be seen at lithospheric depth and hence play a role in the deformation history of the lithosphere.

2. Data and Methods

2.1. Ambient Noise Interferometry

Seismic noise interferometry can be used to measure surface-wave dispersion (Lobkis & Weaver, 2001; Shapiro & Campillo, 2004; Snieder, 2004), and has been successfully implemented in regional and global imaging studies (Lin et al., 2006, 2008; Shapiro et al., 2005). The basic principle behind this method is intuitively demonstrated in Wapenaar et al. (2010): The empirical Green's function representing frequency dependent travel-time between two seismic stations is estimated by cross-correlating the recordings from the stations and stacking this cross-correlation function over an extended period of time (12–24 months). This method helps to avoid the dependence on, and uncertainty of earthquake source parameters used in ballistic surface wave analysis. To build a 3D shear-wave velocity model we measured Rayleigh phase velocities in the 15–95 s band by cross-correlation of ambient noise seismic data. The surface-wave dispersion allows us to construct a both laterally and vertically varying seismic shear-velocity model.

2.2. Processing and Inversion Workflow

The data analyzed in this study were recorded by 566 stations from the USArray network, the Mexican National Seismic Network and several stations located on Cuba and the Cayman Islands. We cross-correlated the vertical component of the noise field in a wide band of frequency between 15 and 95 s (0.0105–0.0667 Hz). This combined data set (Figure 1) ensures sufficient areal coverage of the study area and allows for modeling to depth of 200 km such that we can image a large extent of the upper-most mantle (Figure 2a). Our general processing workflow is adapted from Bensen et al. (2007). The recording from each station was divided into 24-hr segments. Daily cross-correlation functions were calculated between station pairs that have overlapping records. Most of the permanent stations in the data set have been in operation for more than a decade while the temporary networks provide records for a period between 1 and 2 years. For each station pair, all available daily cross-correlation functions were linearly stacked to produce a final cross-correlation function. Filtered empirical Green's functions were extracted from this function using the frequency-time analysis method (Dziewonski et al., 1969; Levshin

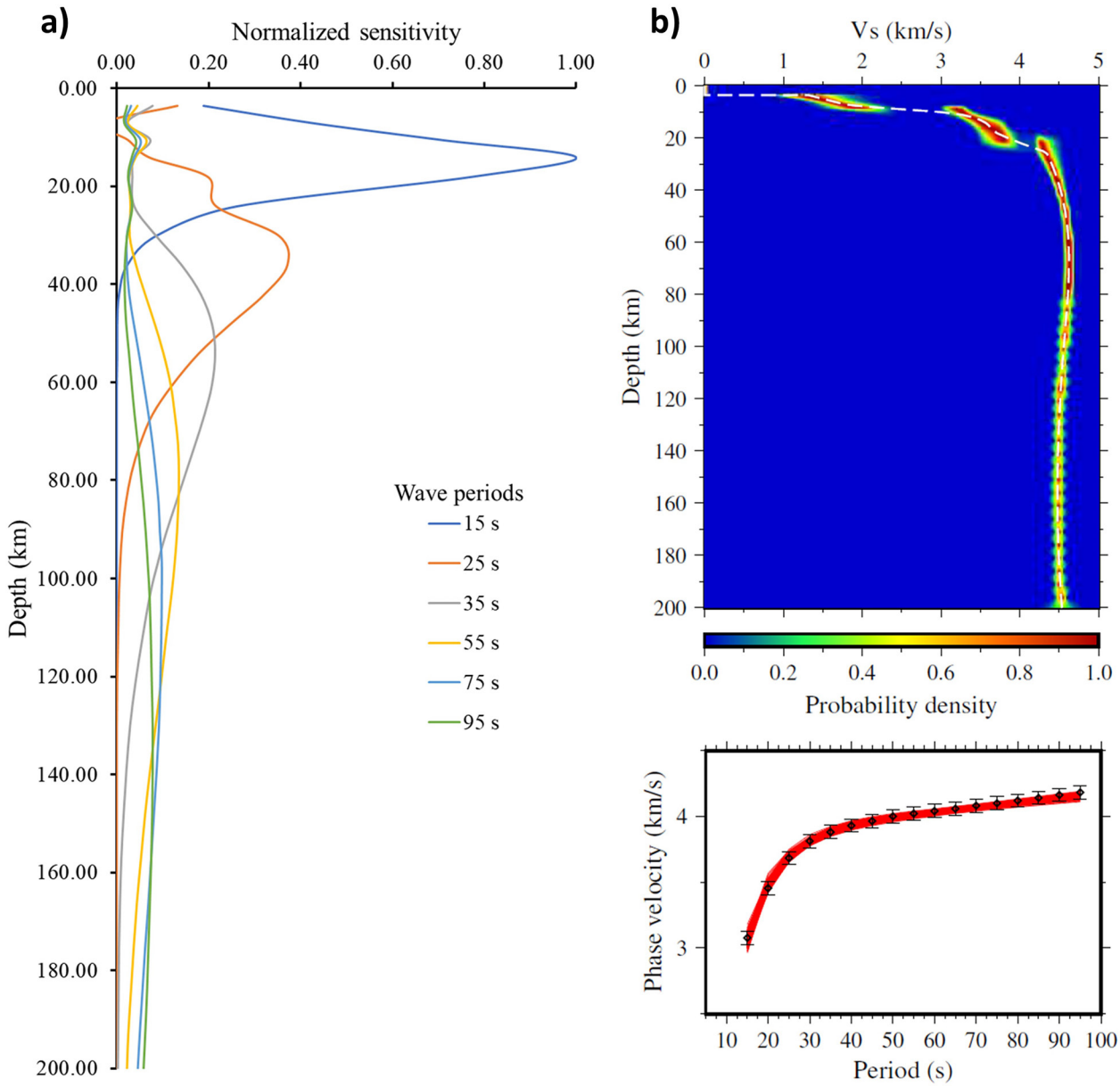

Figure 2. (a) Sensitivity kernel estimating depth coverage of Rayleigh surface-wave across a band of frequency used in this study. (b) Example of an inverted 1D velocity profile (top panel) that produces a good fit (red lines in bottom panel) to a measured dispersion curve (markers with error bars in bottom panel). Color-shaded zone in top panel represents the accepted 1,000 solutions whereas the white dashed line marks the final model calculated from the average of accepted models.

& Ritzwoller, 2001). Only correlations with a signal-to-noise ratio greater than 10 were accepted. This criterion helps to ensure that the uncertainty in phase-velocity measurement is within 35–50 m/s or ~1% (Bensen et al., 2007). Overall, this configuration provides a maximum of 34,166 acceptable empirical Green's functions for the wave period at 20 s and a minimum of 1,635 ray-paths at 95 s. Using these measurements of average phase-velocities, we performed 2D phase-velocity tomography on a half-degree grid with a total of 1,591 nodes that achieved results with sufficient resolution (Figure S1 in Supporting Information S1). While running the tomography, several combinations of the damping and smoothing factors were tested, and we chose a set of parameters that helps to minimize raypath artifacts in the final output. The calculated phase-velocity maps at various frequencies are shown in Figure S2 in Supporting Information S1. At each grid node, the calculated phase-velocity was inverted for a 1D shear-wave velocity profile (Figure 2b) using a Monte Carlo Markov Chain inversion (Afonso et al., 2013; Li et al., 2016). The inversion selected the best 1,000 models from a total of

240,000 random simulations. Model misfits could vary within 1% of the measured phase-velocities. The final shear-wave velocity profile is the average of the accepted models. The initial 1D model is parameterized with one layer of sediment, two layers of crystalline crust, and four layers of mantle. Shear-wave velocity in the sediment can vary between 1.5 and 2.4 km/s with a Vp/Vs ratio of 2.0. Sediment thickness is adopted from published sources (Laske & Masters, 1997; Pindell et al., 2016; Rosenthal & Buffler, 1990; Whittaker et al., 2013). The crystalline crust has a shear-wave speed in the range of 3.0–3.9 km/s and Vp/Vs of 1.75. Initial depth to the base of the crust, or the Moho, is averaged from gravity inversion (Nguyen & Mann, 2017) and the Crust 1.0 model (Laske & Masters, 1997). Due to the lack of high frequencies ($f > 0.0667$ Hz) data, velocity within the crust is constrained to increase with depth. Shear-wave speed varies between 4.2 and 4.8 km/s in the mantle with Vp/Vs of 1.80. A low-velocity zone (LVZ) at the depths 130–160 km is a robust feature in multiple iterations of the unconstrained inversion (Figure S3 in Supporting Information S1), leading us to impose a layer of low velocity (4.40–4.60 km/s) in the final inversion based on a global compilation of the mantle LVZ (Nettles & Dziewoński, 2008). During the inversion, the sediment thickness was allowed to fluctuate within 1 km from the initial input whereas Moho depth can be within ±4 km of the starting model. The final 3D shear-wave velocity model is computed by interpolating all 1D models over the grid.

3. Results

3.1. Shear-Wave Velocities and Crustal Thickness

Our velocity model produces an overall good fit (<1% misfit) to the measured phase velocity (Figure S4 in Supporting Information S1). Shear-wave velocities (Vs) at different depths are shown in Figure 3. The prominent slow Vs body (~3.2 km/s) observed at 15-km depth mostly reflects the thick layer of sediment, which reaches a maximum of ~15 km along the US Gulf Coast margin (Buffler & Sawyer, 1985). At 25-km depth, shear-wave velocity exceeds 4.2 km/s in the center of the ocean basin. This area closely follows the trend of the extinct spreading system imaged in this region of the GOM (Sandwell et al., 2014). Hence, the high Vs here represents the upper most mantle under the thin oceanic crust of the GOM. At 35 km, the high Vs corresponds to mantle under thin crust, and low Vs corresponds to areas of thick crust (Figure 3c). At greater depths (Figures 3d–3f) the velocity fields become more uniform with narrower Vs ranges, all reflecting mantle. Nonetheless, regions of pronounced low velocity (<4.52 km/s), about −2% velocity perturbation, can be observed under northeastern Mexico and offshore the northwestern US Gulf Coast. Slow shear-wave anomalies in northern Mexico have been observed in previous studies (Gaite et al., 2012, 2015; Zhu et al., 2020), which identify the anomalies as fluid-induced melting in the back arc of the Rivera and Cocos subduction beneath the North American plate. The slow anomaly offshore Texas and eastern Mexico can be seen to persist to depth greater than 100 km, albeit with a decreasing amplitude.

Depth to the base of the crust or the Moho is estimated using the 4.2-km/s contour from our 3D Vs model. Comparison between the inversion result and the initial Moho input yields a mean difference and root-mean-square standard deviation of 4.03 and 5.60 km, respectively. We further examined the reliability of our result by matching velocity profiles with Moho depths determined in previous active seismic studies (Figure S5 in Supporting Information S1). Our model shows a close match with GUMBO refraction results where the average difference in Moho depth along four profiles is 2.5 km. The onshore US Gulf Coast Moho is also comparable to that estimated from a joint-inversion study of Miao et al. (2022) with an overall difference of 2.7 km. Figure 4 displays thickness of the crystalline crust taken as lying between the 3.2 and 4.2 km/s contours of our velocity model. The most prominent area in this map is the zone of thin crust (<10 km) with thickness ranging between 5 and 10 km in the center of the GOM basin. The mean thickness of this zone is 7.7 ± 1.2 km, comparable to the 7.08 ± 0.78 km mean thickness of oceanic crust in the Pacific and Atlantic oceans (White et al., 1992). Moving landward into the offshore margins, crustal thickness increases to above 20 km. The onshore US Gulf Coast margin shows thickness of about 20–28 km while the crust is a few kilometers thicker on average under the Yucatan margin. These values are close to the expected 28-km thickness for extended continental crust (Christensen & Mooney, 1995), although our results over the US Gulf Coast margin suggest a higher degree of extension and thinning than the C&M average. The crystalline crust exceeds 40 km in thickness further inland north of the Ouachita Fold Belt as well as under most of inland Mexico outside of the Yucatan peninsula. This is consistent with the 40-km global average for thickness of continental shields and platforms (Figure 5).

10.1029/2022GC010566

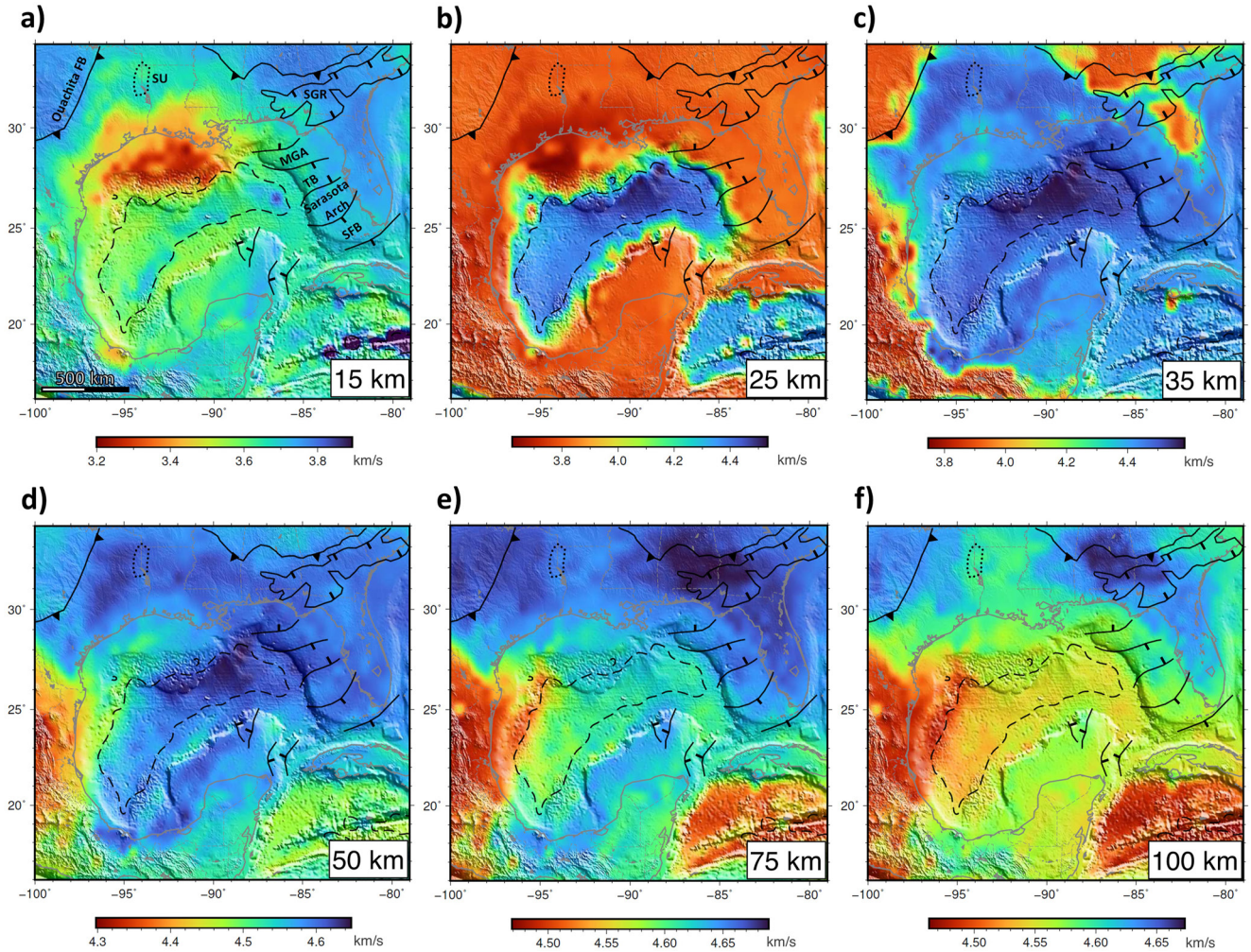

Figure 3. Inverted shear-wave velocities shown at various depths. MGA: Middle Grounds Arch, SFB: South Florida Basin, SGR: South Georgia Rift, SU: Sabine Uplift, and TB: Tampa Basin. Dashed outline in the center is the 10-km thickness contour of crystalline crust computed from our model. The average crustal thickness inside this contour is ~7.8 km.

3.2. Shear-Wave Velocities in the Mantle Lithosphere

Figure 6 shows shear-wave velocities along three profiles crossing the GOM from onshore the US Gulf Coast margin to the southern Yucatan margin. In each profile, the vertical extent of the crystalline crust is marked by the white dashed lines (Figure 6 top panels) capturing the apparent thinning of crystalline crust toward the ocean basin where its thickness reaches a minimum of ~7 km. The lower panels in Figure 6 display Vs variations for the entire upper 200 km along the profiles. Velocities at shallow depths are saturated at 4.4 km/s. Overall, there is a consistent trend of increasing velocity from 4.4 km/s below the crust to >4.6 km/s at about ~75-km depth. Shear velocity then monotonically drops to <4.5 km/s at depth ~160 km. Overlaid on these profiles are the depths at which the velocity decreases most abruptly. This depth has been used as a proxy to determine the lithosphere-asthenosphere boundary (LAB) (Fischer et al., 2010; Palomeras et al., 2017) and here we adopted this definition to define the base of the lithospheric lid. It is clear from these profiles that the LAB separates a fast lid with maximum velocity of 4.65 km/s from a zone of low shear-wave velocity of 4.45 km/s centered at 160 km. This structure of a fast lid above a LVZ in the upper mantle is similar to observations over old oceanic lithospheres (Gaherty et al., 1999; Kawakatsu et al., 2009). Across the three profiles in Figure 6, the LAB exhibits a depth range between 87 and 100 km. The shallowest LAB is observed under the central GOM ocean basin while the deepest LAB is located under the onshore US Gulf Coast, north of the Ouachita Fold Belt. Above the LAB, the velocity structure of the mantle lithosphere also exhibits a consistent pattern such that the lithospheric mantle can be separated into three distinct regions laterally along these parallel profiles: (a) Areas underlying

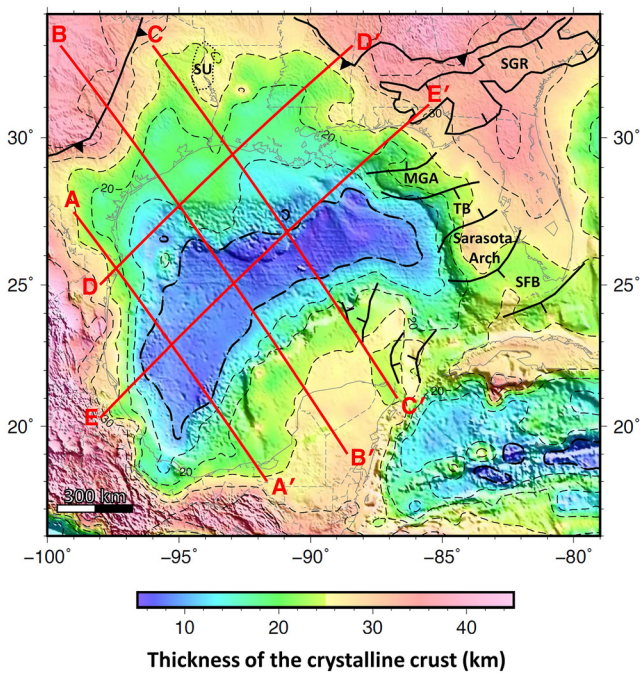

Figure 4. Thickness between the inverted 3.2 and 4.2 km/s contours representing that of the crystalline crust. The 10-km thickness contour (thick dashes) denotes the maximum landward limit of oceanic crust. Red lines mark locations of 2D profiles shown in Figures 6 and 7. MGA: Middle Grounds Arch, SFB: South Florida Basin, SGR: South Georgia Rift, SU: Sabine Uplift, and TB: Tampa Basin.

thick crust with high Vs of >4.65 km/s (+2% Vs perturbation), (b) Areas underlying oceanic crust with Vs of ~4.6 km/s, the average Vs in this depth range, and (c) The lithospheric mantle below the offshore US Gulf Coast area where the crust is between 10 and 20 km in thickness and mantle velocities are <4.53 km/s, below the mean (−2% Vs perturbation).

These persistent correlations of crustal thickness, LAB depths and lithospheric mantle velocity are used to delineate different tectonic provinces along the profiles as labeled in Figure 6. The narrow region of thin crust (<10 km) above the mantle lid of intermediate Vs (4.55 km/s) underlain by a shallow LAB is interpreted as oceanic crust and lithosphere. Regions with deep LAB, 95–100 km, are mostly associated with unstretched or slightly stretched continental lithosphere with crustal thickness greater than 30 km and high mantle-lid velocity (4.65 km/s). Regions with the LAB at 90-km depth correspond with extended crust, 10–20 km in thickness, and slow mantle-lid Vs of <4.53 km/s. We interpret this area as highly extended and deformed continental lithosphere. The contrast between the oceanic and highly extended continental lithospheres is further illustrated in Figure 7. Profile D-D′ (Figure 7a) traverses mostly over region of extended continental lithosphere whereas the subparallel profile E-E′ (Figure 7b) samples a large swath of oceanic lithosphere. Relative to E-E′, profile D-D′ shows thicker crust, lower average Vs in the mantle lithosphere and a deeper LAB.

Using the derived crustal thickness model, we calculated two attributes related to extension over the GOM region: the stretching or beta-factor and the extension length. Beta-factors are mapped as the ratio between the nominal pre-rift thickness (40 km) and the current estimated thickness of the continental crystalline crust with 1 being no stretching (Figure 8a). There is a clear asymmetry in crustal structure between the conjugate US Gulf Coast and Yucatan margins. The Yucatan crust is thicker on average and has a narrower transition from the continental to oceanic domain. On the Yucatan side, the transition from beta factor 2 to 3 takes place over a distance of <150 km whereas the same transition occurs over more than ~300 km over the conjugate US Gulf Coast margin. The reduced velocity in the mantle lithosphere associated with the highly extended terrain is observed only under the US Gulf Coast margin and not its conjugate. In addition, this zone of highly extended lithosphere features an eastward trend in which it becomes narrower in its extent and slightly higher in its shear-wave velocity. This pattern can be observed from profiles A-A′ through C-C′. Comparing the highly extended zone along profile A and that of profile C shows that its width decreases from 540 to 300 km and its average velocity increases from ~4.53 to ~4.62 km/s. The animation in Figure S6 in Supporting Information S1 more clearly illustrates this subtle but rather consistent pattern moving from west to east across the US Gulf Coast margin. As discussed in Section 4.1, we interpret this lateral variation in velocity of the mantle lithosphere as a reflection of an eastward decrease in extensional deformation controlled by pre-rift lithospheric thickness.

3.3. Depth to the Lithosphere-Asthenosphere Boundary

The variation in LAB depth reflects the distribution of various tectonic terrains within the GOM area (Figure 9). For example, the seaward shallowing LAB follows the transition from the continent, through the extended terrain, to the oceanic lithosphere. Since the surface-wave method is not sensitive to sharp velocity discontinuities nor is it likely that the LAB is a sharp transition, we compared our estimate of depth to LAB with that of other studies for the onshore US Gulf Coast. For most of Texas, our average LAB depth of 90 km is comparable to the 80–95 km range derived from receiver function measurement of Abt et al. (2010). Over the southeastern US, our LAB depth of 97 km is consistent with their 95–100 km range. Our oceanic 87-km LAB is also in agreement with the 87-km LAB depth calculated for old oceanic plate (>150 Ma) in the Pacific (Schmerr, 2012). Nevertheless, the model from Sp receiver function of Ainsworth et al. (2014) along a 2D profile across the onshore Texas US Gulf Coast shows the top of a thick lithosphere-asthenosphere transition zone that is 10–20 km deeper than our LAB estimate.

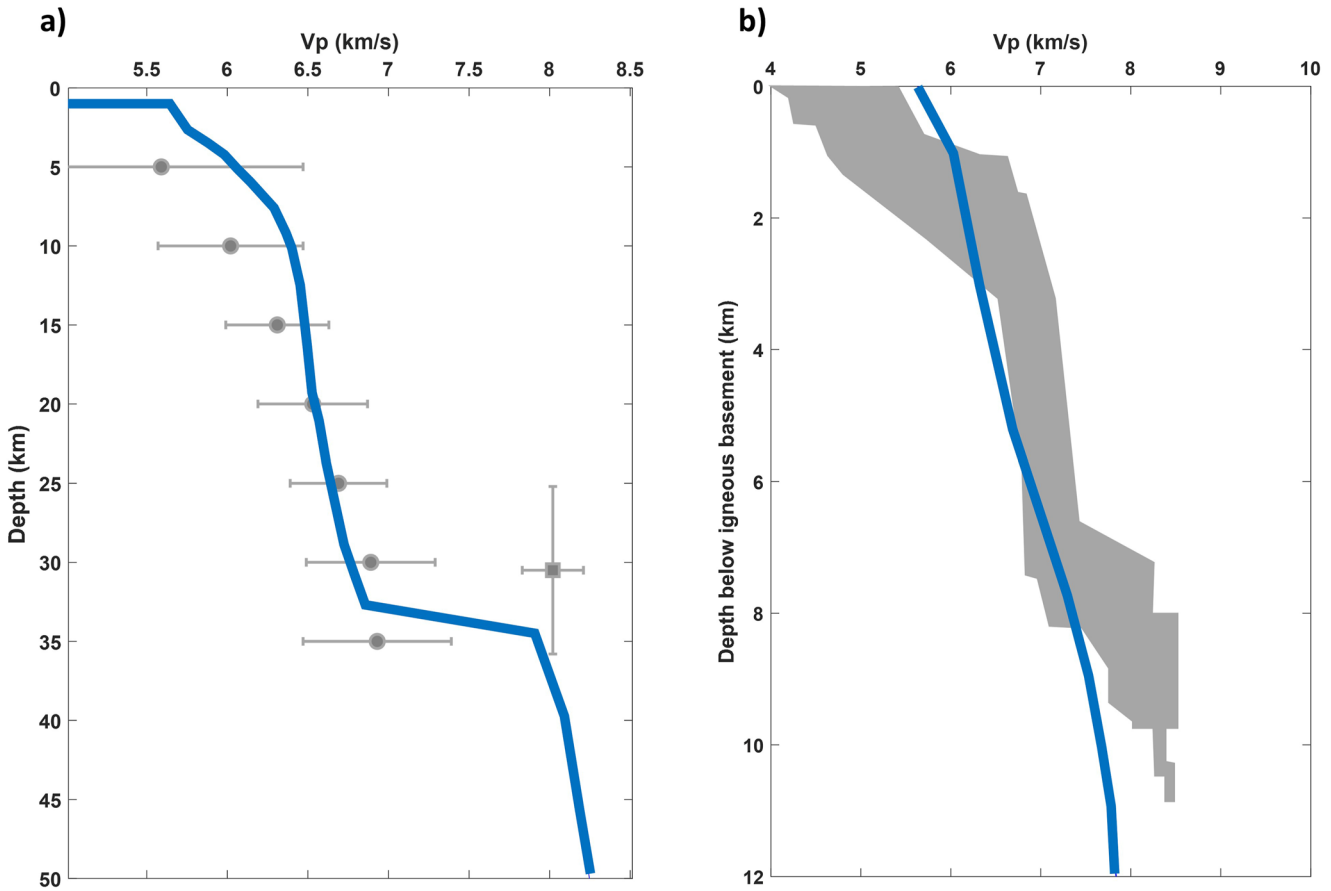

Figure 5. (a) Average velocity profile for continental crust from our study (blue line) in comparison to the global average (Christensen & Mooney, 1995) shown by circle markers with their standard deviations. Square marker is the global average of Moho depth. (b) Average velocity profile for oceanic crust from our study (blue line) in comparison to the value ranges (gray shade) observed from the Atlantic and Pacific Oceans (White et al., 1992). *P*-wave velocity is derived from *S*-wave velocity using 1.75 conversion factor.

Given the large vertical resolution (~25 km) inherent in surface wave method and the probable gradational nature of the LAB, it is a challenge to resolve the LAB depth unambiguously. Rather than looking at the absolute LAB depths, we find the consistent trend of LAB across different geologic domains in our study area more insightful. Using our estimated LAB depth, we computed the beta factor for the mantle lithosphere, assuming a pre-rift

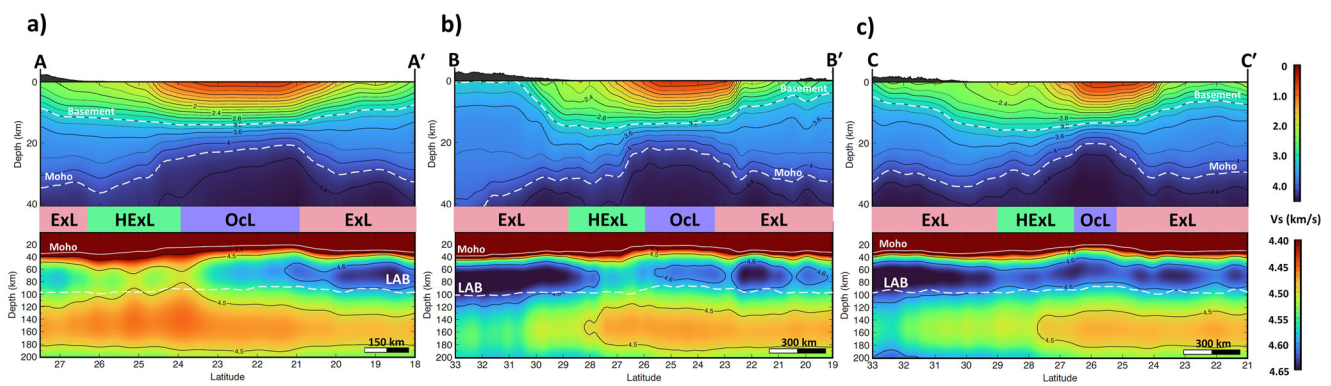

Figure 6. Shear-wave velocity across three northwest-southeast profiles shown in Figure 4 at crustal (top panels) and lithospheric (bottom panels) scales. The vertical extent of igneous crust is bounded by the white dashed lines (top panels). In the lower panels, velocity at shallow depth is saturated at 4.4 km/s. ExL: Extended lithosphere, HExL: Highly extended lithosphere, OcL: Oceanic lithosphere, and LAB: lithosphere-asthenosphere boundary.

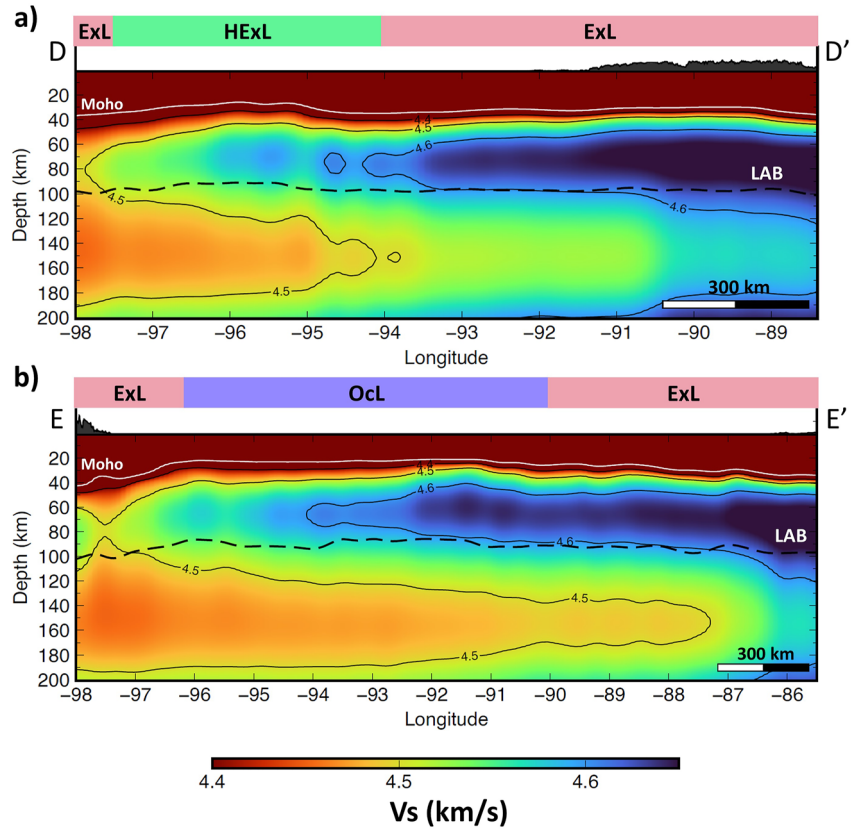

Figure 7. Shear-wave velocity across the northeast-southwest profiles shown in Figure 4 at lithospheric scale. Velocity is saturated at 4.4 km/s. Profile D-D′ mostly samples highly extended and extended continental lithosphere (a) while profile E-E′ traverses a large swath of oceanic lithosphere. ExL: Extended lithosphere, HExL: Highly extended lithosphere, and OcL: Oceanic lithosphere.

thickness of 70 km (110 km for whole lithosphere) (Figure 8b) and observed a stark contrast in comparison to the stretching factor of the crust. The mantle lithosphere shows very little sign of extension, $\beta \sim 1.1$, even though the crystalline crust has been extended significantly, $1.5 < \beta < 3$. While depth-dependent extension is commonly seen at rifted margins where the mantle lithosphere usually displays a higher degree of extension than the crust, the contrast observed in the northern GOM margin is too extreme to be explained by these models. Thus, we interpret that like the crust, mantle lithosphere was thinned substantially during rifting but has since regained its thickness by incorporating the underlying asthenosphere through conductive cooling (Stein & Stein, 1992).

3.4. Differential Stretching Along the Continental Margins

To compute the extension length across both the US Gulf Coast and Yucatan margins, several NW-SE 2D profiles were constructed with one end at a location of beta-factor ~1 and the other end at the continent-ocean boundary (Minguez et al., 2020). Along each profile, the total area of the crystalline crust was calculated. This area is used to restore the margin to a point where the crystalline crust has a uniform thickness of 40 km. The white dots in Figure 8a mark the restored points along the US Gulf Coast margin. To account for its counterclockwise drift during the Jurassic seafloor spreading, the YB needed to be reconstructed back to its pre-drift location before the amount of extension across the Yucatan margin could be measured along the direction of rifting. We rotated the YB back along the pole determined by Nguyen and Mann (2016). The beta-factors along the northern US Gulf Coast margin show a notable contrast between its western and eastern regions. In the northwestern GOM, the transition between area of beta-factor ~1 to beta-factor >3 occurs over a distance of ~270 km whereas a similar transition covers more than 600 km on the eastern side. The total amount of extension length increases by ~140 km from west to east. This suggests that the spatial and temporal rates of extension were higher in the northwestern margin. While seafloor-spreading initiated in the western GOM, most of the eastern section was still

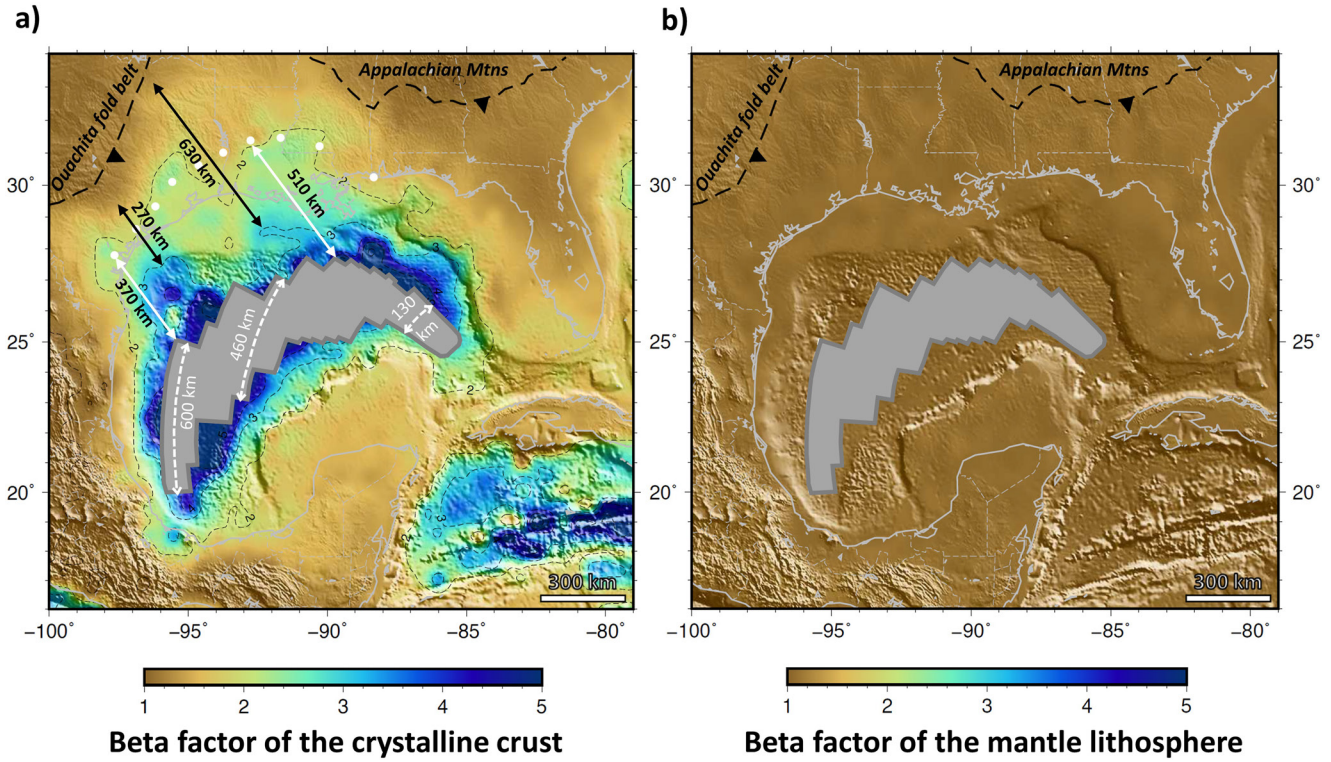

Figure 8. (a) Stretching beta factor of the crystalline crust calculated as the ratio between an original thickness of 40 km and the currently observed thickness. Gray-shaded region is underlain by oceanic crust (Minguez et al., 2020). White dots mark the reconstructed margin after restoring the crust to a uniform 40-km thickness in a northwest-southeast direction (solid arrows). Extension length increasing from west to east along the US Gulf Coast margins is illustrated by the two white solid arrows. Black arrows mark the distances between areas with beta factor ∼1 to those with beta factor of 3. Dashed arrows depict maximum amount of seafloor spreading in the western Gulf of Mexico decreasing eastwardly. (b) Stretching beta factor of the mantle lithosphere calculated using 70-km as its pre-rift thickness. Note the large contrast in beta factors between the crust and mantle lithosphere suggesting thermal thickening of the lithosphere since breakup.

undergoing continental extension for quite some time. This west-east migration of seafloor spreading has been well established (Minguez et al., 2020; Pindell et al., 2021) and is evident in the area of oceanic crust observed in the central GOM basin. The amount of the ocean floor generated by the westernmost extinct-spreading center is ∼600 km wide whereas the easternmost extinct ridge produced roughly 150 km of crust (Figure 8). We discuss possible scenarios that lead to earlier breakup in the western GOM in Section 4.2.

4. Discussion

4.1. Origin of the Reduced Velocity in the Mantle Lithosphere

Here we discuss a few mechanisms under which a LVZ can form within the lithospheric mantle, including the effects from thermal anomaly, extensional deformation, and intrusion of melts. Although each of these processes is considered individually, they are not necessarily mutually exclusive. Slow seismic velocity anomalies at depths of 50–400 km in the northwestern GOM vicinity have been reported previously (Krauss & Menke, 2020; Yao & Li, 2016; Zhu et al., 2020). A deep thermal anomaly represented by slow Vs at 250-km depth as well as a shallower (50–150 km) low Vs body were imaged by teleseismic tomography centered around 92°W and 29°N (Krauss & Menke, 2020). Rayleigh ambient noise tomography from Yao and Li (2016) imaged a small negative Vs anomaly at depth of 50 km beneath the onshore coast of Texas. Also, teleseismic study onshore Texas (Evanzia et al., 2014) detected low Vs from 40 to 200 km below the US Gulf Coast. Zhu et al. (2020) performed full-waveform inversion for the entire Middle America and captured a slow Vs anomaly between 200 and 400-km depth, centered at 96°W 25°N in the northwestern GOM. This anomaly appears to directly overlie the subducted Rivera slab, and it might be associated with the mantle wedge seen in subduction zones under a back-arc (Wiens et al., 2008). Although based on its location, this mantle anomaly seems unlikely to be related to the anomaly reported by Krauss and Menke (2020), presence of a subduction-induced upwelling could heat

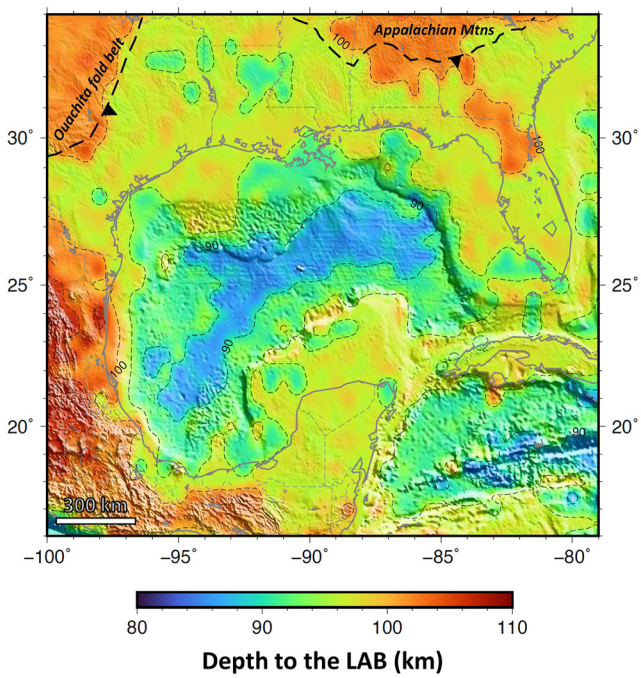

Figure 9. Depth to the lithosphere-asthenosphere boundary calculated as the depth of maximum negative gradient of the 1D shear-wave velocity.

the overlying lithosphere and thus reduces its shear-wave velocity. In fact, a model of the GOM opening as a back-arc basin has been proposed based on its location directly behind the volcanic arc in northern Mexico (Stern & Dickinson, 2010). The described eastward trend of increasing velocity in the mantle lithosphere along the northern GOM margin can simply be due to the greater distance from the subducting slab, reducing the effect of the mantle upwelling on the extended lithosphere. However, despite evidence seemingly supportive of low shear-wave velocity in the mantle lithosphere resulting from an asthenospheric thermal anomaly, several observations work against this hypothesis. The aforementioned low Vs anomalies at depth below 200 km imaged from previous studies do not exhibit signs of upwelling that can affect the thermal state of the shallower lithosphere at 100-km depth. This observation is further supported by analysis of our velocity model. We used the derivative relationship between temperature and shear-wave velocity of -3.75×10^{-4} km s^{-1} °C^{-1} (Liu et al., 2005; Priestley & McKenzie, 2006) to examine to likelihood of a thermally induced Vs reduction. The result shows that the Vs anomaly observed within the mantle lithosphere would imply a thermal anomaly with magnitude of >150°C at depth 75 km. A thermal anomaly on this scale at shallow depth seems unrealistic in a passive margin where rifting has ceased for more than 150 million years. Therefore, the observed reduction in Vs in the northwestern GOM is unlikely to be associated with an anomalous mantle heat source. The velocity-reducing effect of fluid-induced melting usually associated with a subducting slab is also not considered due to the lack evidence for widespread melt intrusion at the crustal level.

Mantle rock under stress during extension can be weakened due to grain-size reduction (Karato & Wu, 1993; Yamasaki, 2004). Such weaker rocks at smaller grain size would exhibit a reduced shear-wave velocity (Faul & Jackson, 2005; Jackson et al., 2002). Hence, extensional deformation during Triassic-Jurassic rifting could be a viable mechanism under which the mantle lithosphere of the northern GOM margin became weaker, resulting in a drop in its shear modulus that is manifest as zone of reduced Vs. The observed eastward increase in mantle Vs then represents a decreasing degree of mantle deformation from west to east. The combination of continuing extension and grain-size reduction could lead to diffusion-creep behavior of the mantle lithosphere (Karato & Wu, 1993) that promotes strain-weakening. Hopper and Buck (1993) showed that deformation under the diffusion-creep regime would enable the lithosphere to begin deforming at a stress-level that is lower than otherwise required and thus further enhance rifting. This positive feedback loop between extension and grain-size reduction would ultimately lead to rapid breakup in the western side of the northern GOM margin as compared to its eastern counterpart.

Decompression melting at the top of the asthenosphere as the lithosphere was stretched and thinned during rifting could generate melts that infiltrated the overlying mantle lithosphere. Partial melts can reduce the Vs of the aggregates but due to their lower density at depth within the lithosphere they are expected to rise through the lithosphere, intrude the crust and/or erupt as lava. In that case, the negative effect on Vs of partial melts would only be transient. However, if the melts are trapped in the mantle lithosphere (Müntener et al., 2009; Pérez-Gussinyé et al., 2006) metasomatic reaction with the host rock will take place. This is a process of mantle refertilization during which the depleted harzburgite in the lithosphere is enriched and become lherzolite (O'Reilly & Griffin, 2013). As a result, the mantle lithosphere becomes denser but has a lower seismic velocity, a weaker rheology and a smaller elastic thickness. Evidence from petrological studies shows that mantle metasomatism has occurred in both cratonic (Casagli et al., 2016; Griffin et al., 2009; Wang et al., 2015) and off-cratonic environments as well as in oceanic regions (O'Reilly & Griffin, 2013; Piccardo, 2008). Using a compilation of available petrological data from Alpine-Apennine ophiolites, Piccardo (2008) constructed a model for the opening of the ancient Ligurian Tethys ocean basin. In that model, both the extended continental lithosphere surrounding the ocean basin and the oceanic lithosphere itself experience metasomatism due to melt percolation. In the GOM, evidence for rejuvenation of the mantle lithosphere during Mesozoic rifting was found in crustal xenoliths collected along the coast of Louisiana (Stern et al., 2011). Radiometric dating confirms the age of these samples

at ~160.1 Ma, approximately close to the time of breakup. Furthermore, trace element analysis indicates a history of mantle enrichment and low-degree of melting, raising the possibility of mantle metasomatism due to melt-rock interaction during the Mesozoic extension. It is likely that the observed Vs reduction from our model results from the combined effects of extensional deformation and mantle refertilization during rifting.

4.2. Deformable Plate Modeling

While the counterclockwise rigid motion of the YB is sufficiently constrained by the geometry of the imaged seafloor spreading fabric (Minguez et al., 2020; Nguyen & Mann, 2016), the direction of extension during continental rifting is not well defined. This lack of constraint has resulted in various reconstruction models that restored the YB along different trajectory for the rifting periods. The relative extension between the YB and North America has been predicted as toward the southeast (Marton & Buffler, 1994; Miao et al., 2022), along a counterclockwise rotation (Dunbar & Sawyer, 1987), and almost due south (Kneller & Johnson, 2011). Here, we constructed deformable plate models in conjunction with our derived crustal thickness to evaluate these end-member cases and constrain the direction of extension. A plate model helps predict distribution of crustal thickness corresponding to a distinct opening direction. Using our derived crustal thickness as a proxy, different plate models for the rifting phase can be examined.

Deformable plate modeling is carried out in GPlates application (Müller et al., 2018). Its underlying algorithms were developed using Delaunay Triangularization and Barycentric coordinates interpolation (Gurnis et al., 2018). A triangular mesh is generated over a region of future deformation. As extension proceeds, the mesh expands along with the deformed region and tracks changes in crustal thickness at individual Lagrangian points. Stretching a geologic body in different directions would lead to different distribution of its final thickness after extension. Figure 10 shows the predicted crustal distribution at the end of continental rifting (~158 Ma) from three scenarios in which the Yucatan moved away from North America in different directions (arrows in Figures 10b–10d). These results are compared to our crustal thickness derived from the inverted Vs model (Figure 10a) which serves as the observed thickness in these tests. In the first two cases in which extension takes place in the north-south and counterclockwise directions (Figures 10b and 10c), respectively, crustal thickness displays a trend of thinning toward the east with a noticeably thickened crust in the southwestern region whereas the thinnest crust is located at the southeastern corner. These features are not observed in the inverted crustal thickness (Figure 4). Moreover, the observed thinned crust offshore Texas and Louisiana (Figure 10a) is mostly absent from these models. On the other hand, the last scenario with a southeast extension (Figure 10d) produces a result that is more comparable to the observation. The overall thinning is toward the south. The thinnest crust observed offshore Texas and Louisiana is similar to our inverted model. A NW-SE extension is also favored by quantitative correlations. In comparing the crustal thickness at individual grid points from the plate models to that of the inverted model, extending the margin toward the southeast produces the smallest mean and RMS errors of 4.06 and 5.27 km, respectively. The other two cases generated errors several times as large (Figures 10b and 10c). These analyses suggest that the Mesozoic continental rifting occurred predominantly toward the southeast with respect to North America. This is in agreement with recent analyses of crustal thickness and seismic velocity in the mantle lithosphere (Miao et al., 2022; Nguyen et al., 2022).

4.3. A Model for the Continental Rifting and the Opening of the GOM

Our results show that the rate of crustal extension was highest over the northwestern GOM margin and gradually decreased toward the east (Section 3.4). The difference between narrow and wide rifts is controlled by the strength of the deforming lithosphere, in that a cold and strong lithosphere leads to a narrow rift zone whereas warm and weak lithosphere favors a wide rift zone (Buck et al., 1999; Corti et al., 2003; Gueydan et al., 2008; Kogan et al., 2012). From our model and previous studies, several parameters exhibit an eastward trend along the US Gulf Coast margin including more gradual crustal extension, delayed breakup, lower degree of velocity reduction in the mantle lithosphere, and increasing amount of volcanic and magmatic emplacement. A rifting model in which the extension took place over a lithosphere with different inherited thickness can help to explain these observed trends (Figure 11). In such a model, initial rifting was widely distributed along the entire US Gulf Coast margin (Figure 11a). However, extension became localized along a shear-zone which developed as the mantle lithosphere was weakened by melt refertilization (Figure 11b). This is similar to the "weak seeds" often imposed in thermomechanical models in order to initiate a localized shear-zone (Huismans & Beaumont, 2007).

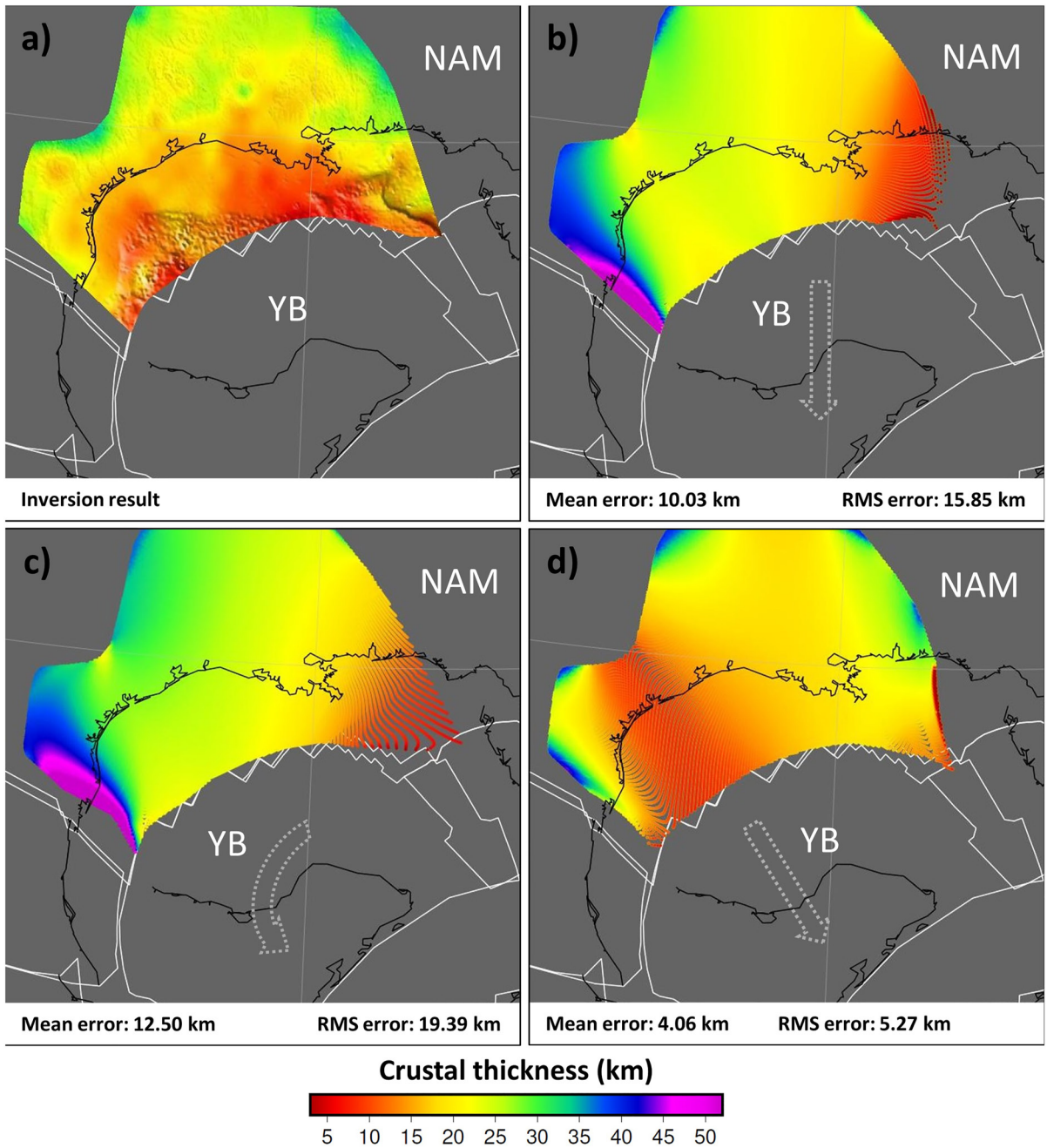

Figure 10. Deformable plate modeling is used to predict the distribution of crustal thickness at 158 Ma, presumably the end of rifting, as a function of rifting direction (dashed arrows). Limit of extended crust associated with rifting (colored area) is estimated from our calculated crustal thickness map (Figure 4). Of the three scenarios tested, a southeastern motion (d) of the Yucatan block away from the North American plate during continental extension produces the smallest errors with respect to our inverted crustal thickness (a).

The development of a large-scale ductile shear-zone could have contributed to mantle exhumation observed in the northwestern GOM margin (Van Avendonk et al., 2015). This process was enhanced there likely due to the greater thickness of the pre-rift continental lithosphere in this part of the margin. The thick lithosphere hindered the upward migration of asthenospheric melt through the overlying mantle lithosphere of the extending plate (Korenaga et al., 2002). These trapped melts may have reacted with the lithospheric mantle causing metasomatism that refertilized the mantle lithosphere, weakening it, reducing seismic velocity and elastic thickness. Although any variation in pre-rift thickness of the lithosphere has most likely been erased by the process of rifting, a remnant slab of oceanic lithosphere trapped beneath the Texas coastal plain (Evanzia et al., 2014; Keller &

10.1029/2022GC010566

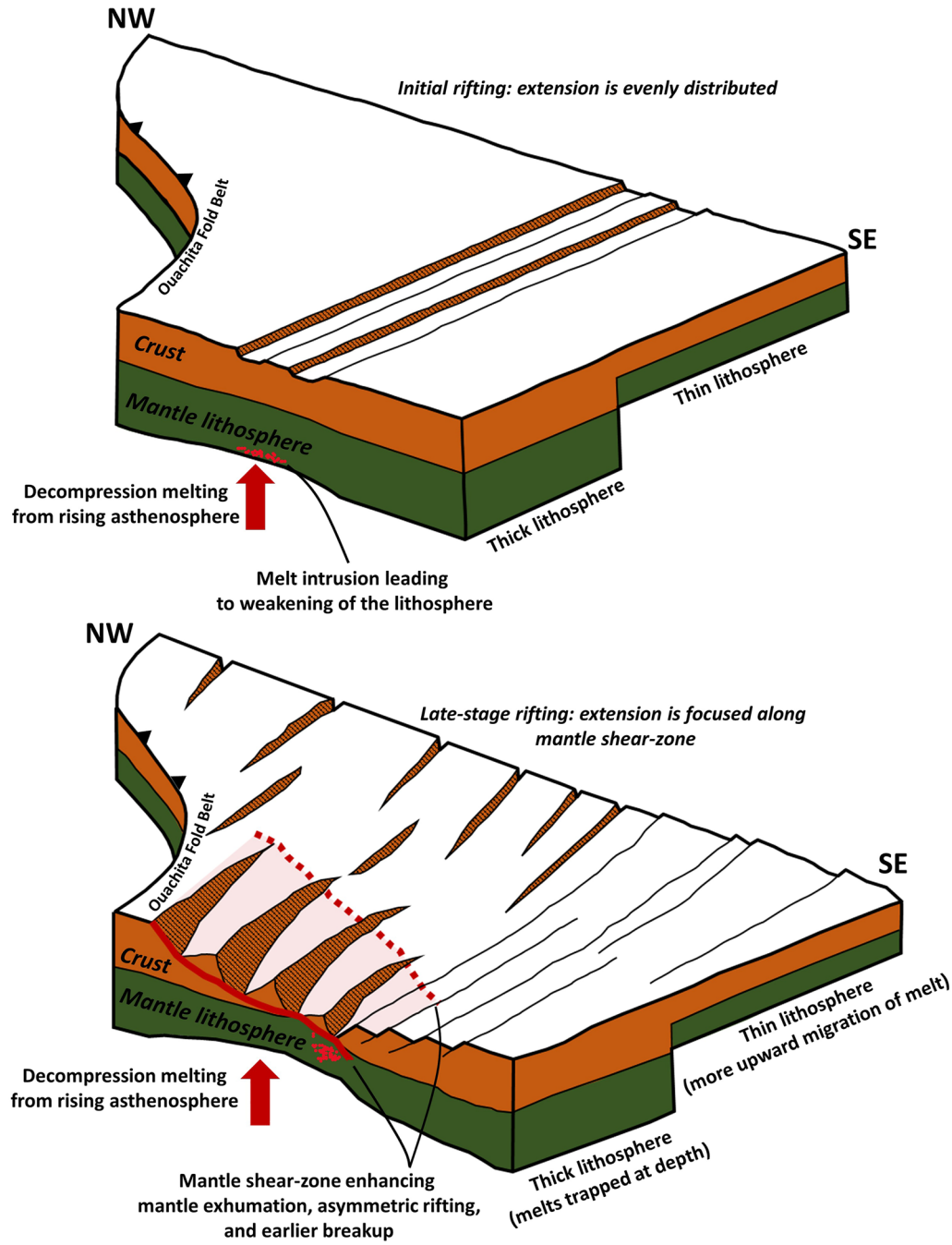

Figure 11. Schematic model proposed for the formation of rifted margins surrounding the Gulf of Mexico (GOM). (a) Symmetric and distributed rifting at the early stage. Thinning of the lithosphere was accompanied by passive asthenospheric upwelling and decompression melting. The eastern part of the plate is inferred to have had a thicker pre-rift thickness that hindered melt migration through the lithosphere leading to refertilization and weakening of the mantle lithosphere. (b) Development of mantle shear-zones led to focused deformation and earlier breakup in the western region. This localized deformation also resulted in asymmetric extension in which most of the thinning took place on the North American margin. The zone of highly extended and deformed mantle lithosphere is now observed as the low Vs region in the northwestern GOM.

Hatcher, 1999; Keller & Shurbet, 1975) could be a potential contributor to an overall thicker plate in the western US Gulf Coast margin prior to rifting.

The development of localized mantle shear-zones led to more rapid extension and earlier break-up in the northwestern GOM margin (Figure 11b). In contrast, the inferred thinner lithosphere in the central and eastern sides of the northern GOM margin produced a wider rift zone that extended for a longer period of time and led to a later start of seafloor spreading. Because of this lateral variation in extensional rate, the YB was forced to drastically change its motion from NW-SE rifting to counterclockwise drifting. Melt migration and extraction was also much more efficient in this region, enhancing syn-rift volcanism and magmatism (Christeson et al., 2014; Eddy et al., 2014, 2018). Without refertilization of its mantle, the present-day lithosphere here is stronger than its western counterpart and exhibits higher seismic velocity and greater elastic thickness (Tesauro et al., 2015). The presence of a major shear zone during rifting would also explain the asymmetry structure across the conjugate margins. In contrast to the observation over the US Gulf Coast margin, there is no evidence for reduced velocities in the mantle lithosphere under most of the Yucatan margin. As we have attributed the slow velocity zone in the lithospheric mantle under the northwestern GOM to melt-induced metasomatism and deformation, this asymmetry between the conjugate margins implies that most melting occurred beneath the northern margin. For this to happen, a shear-zone must have formed that focused deformation and mantle upwelling in the northern part. A southeastward dipping shear-zone would facilitate asymmetric rifting in which the ensuing mantle upwelling would focus only beneath the US Gulf Coast margin where generated melt infiltrated and re-fertilized the overlying lithosphere. This result from our velocity model provides additional support for ductile shear-zones at lithospheric scale that has been suggested as an important feature during continental rifting at other margins (Kelemen & Dick, 1995; Vissers et al., 1991).

5. Conclusions

Measurement of Rayleigh surface wave tomography from ambient noise cross-correlation was used to construct a 3D shear-wave velocity model for the greater GOM region. Our velocity model shows consistent variations in both crustal and lithospheric structures along the northern GOM margin. Within the mantle lithosphere underlying regions of stretched continental crust, we identified a zone of reduced velocity ($\delta v \sim -2\%$) that gradually decreases in amplitude toward the east along this margin. Such a zone is not observed in the mantle lithosphere beneath the conjugate Yucatan margin. We attribute this reduction of seismic wave speed to the combination of deformational grain-size reduction and melt-related mantle metasomatism that weakened the lithosphere during Late Triassic—Early Jurassic rifting. The structural asymmetry between the conjugate northern and southern US Gulf Coast margins suggests a period of extension along a localized shear-zone that focused asthenospheric melt to only the northwestern US Gulf Coast margin. Presence of these mantle shear-zones is supported by the lithospheric boudinage reported in Nguyen et al. (2022). We also mapped out the distribution of crustal thickness and depth to the LAB over the GOM region. The LAB is shallowest at 87-km depth under oceanic domain with average crustal thickness of <8 km. Maximum LAB depth >100 km is found under thick continental regions north of the Ouachita orogen thrust front. Intermediate LAB depth underlies most of the extended continental terrains. We used deformable plate modeling to examine the direction of continental rifting between the YB and the North American plate and determined that extension toward the southeast produced results most consistent with our derived crustal model. The abrupt change in motion of the YB between rifting and drifting can be attributed to the initiation of one or more mantle shear-zone in the western region of the rift zone that led to more rapid extension and earlier breakup.

Data Availability Statement

Broadband seismic records are freely available and can be requested at http://www.ssn.unam.mx/doi/networks/mx/ for the stations from the national network of Mexico, and http://ds.iris.edu/ds/nodes/dmc/forms/breqfast-request for all other stations used in this study including following seismic networks: (a) the TA (Transportable Array; IRIS Transportable Array, 2003); (b) the US (USNSN, Albuquerque Seismological Laboratory (ASL)/USGS, 1990); (c) the IU (GSN; Albuquerque Seismological Laboratory (ASL)/USGS, 1988); (d) the TX (Bureau of Economic Geology, The University of Texas at Austin, 2016); (e) the Z9 (Fischer et al., 2010); (f) the TO (MASE, 2007; VEOX, 2010); (g) the N4 (ASL, 2013); (h) the CU (ASL, 2006); and (i) the CW (National Centre for Seismological Research (CENAIS Cuba), 1998).

Acknowledgments
We thank Xyoli Pérez Campos for her help in accessing the seismic records from the Mexico National Seismological Service. We thank Wenpei Miao for his assistance in initial organizing and processing the data.

References

Abt, D. L., Fischer, K. M., French, S. W., Ford, H. A., Yuan, H., & Romanowicz, B. (2010). North American lithospheric discontinuity structure imaged by Ps and Sp receiver functions. *Journal of Geophysical Research*, *115*(9), 1–24. https://doi.org/10.1029/2009JB006914

Afonso, J. C., Fullea, J., Griffin, W. L., Yang, Y., Jones, A. G., Connolly, J. A. D., & Reilly, S. Y. O. (2013). 3-D multiobservable probabilistic inversion for the compositional and thermal structure of the lithosphere and upper mantle. I: A priori petrological information and geophysical observables. *Journal of Geophysical Research: Solid Earth*, *118*(5), 2586–2617. https://doi.org/10.1002/jgrb.50124

Agrawal, M., Pulliam, J., Sen, M. K., & Gurrola, H. (2015). Lithospheric structure of the Texas-Gulf of Mexico passive margin surface wave dispersion and migrated Ps receiver functions. *Geochemistry, Geophysics, Geosystems*, *16*(7), 538–551. https://doi.org/10.1002/2015GC005803.Received

Ainsworth, R., Pulliam, J., Gurrola, H., & Evanzia, D. (2014). Sp receiver function imaging of a passive margin: Transect across Texas's Gulf Coastal Plain. *Earth and Planetary Science Letters*, *402*(C), 138–147. https://doi.org/10.1016/j.epsl.2014.05.056

Albuquerque Seismological Laboratory (ASL)/USGS. (1988). Global seismograph network - IRIS/USGS [Dataset]. International Federation of Digital Seismograph Networks. https://doi.org/10.7914/SN/IU

Albuquerque Seismological Laboratory (ASL)/USGS. (1990). United States National Seismic Network [Dataset]. International Federation of Digital Seismograph Networks. https://doi.org/10.7914/SN/US

Albuquerque Seismological Laboratory (ASL)/USGS. (2006). Caribbean USGS network [Dataset]. International Federation of Digital Seismograph Networks. https://doi.org/10.7914/SN/CU

Albuquerque Seismological Laboratory (ASL)/USGS. (2013). Central and eastern US network [Dataset]. International Federation of Digital Seismograph Networks. https://doi.org/10.7914/SN/N4

Bensen, G. D., Ritzwoller, M. H., Barmin, M. P., Levshin, A. L., Lin, F., Moschetti, M. P., et al. (2007). Processing seismic ambient noise data to obtain reliable broad-band surface wave dispersion measurements. *Geophysical Journal International*, *169*(3), 1239–1260. https://doi.org/10.1111/j.1365-246X.2007.03374.x

Bird, D. E., Burke, K., Hall, S. A., & Casey, J. F. (2005). Gulf of Mexico tectonic history: Hotspot tracks, crustal boundaries, and early salt distribution. *AAPG Bulletin*, *89*(3), 311–328. https://doi.org/10.1306/10280404026

Buck, W. R., Lavier, L. L., & Poliakov, A. N. B. (1999). How to make a rift wide. *Philosophical Transactions of the Royal Society A: Mathematical, Physical & Engineering Sciences*, *357*(1753), 671–693. https://doi.org/10.1098/rsta.1999.0348

Buffler, R. T., & Sawyer, D. S. (1985). Distribution of crust and early history, Gulf of Mexico basin. *Transactions - Gulf Coast Association of Geological Societies*, *35*, 333–344.

Bureau of Economic Geology, The University of Texas at Austin. (2016). Texas seismological network [Dataset]. International Federation of Digital Seismograph Networks. https://doi.org/10.7914/SN/TX

Casagli, A., Frezzotti, M. L., Peccerillo, A., Tiepolo, M., & De Astis, G. (2016). (Garnet)-spinel peridotite xenoliths from Mega (Ethiopia): Evidence for rejuvenation and dynamic thinning of the lithosphere beneath the southern Main Ethiopian Rift. *Chemical Geology*, *455*, 231–248. https://doi.org/10.1016/j.chemgeo.2016.11.001

Christensen, N. I., & Mooney, W. D. (1995). Seismic velocity structure and composition of the continental crust: A global view. *Journal of Geophysical Research*, *100*(B7), 9761–9788. https://doi.org/10.1029/95jb00259

Christeson, G. L., Avendonk, H. J. A. V., Norton, I. O., Snedden, J. W., Eddy, D. R., Karner, G. D., & Johnson, C. A. (2014). Deep crustal structure in the eastern Gulf of Mexico. *Journal of Geophysical Research: Solid Earth*, *119*(9), 6782–6801. https://doi.org/10.1002/2014JB011045

Corti, G., Bonini, M., Conticelli, S., Innocenti, F., Manetti, P., & Sokoutis, D. (2003). Analogue modelling of continental extension: A review focused on the relations between the patterns of deformation and the presence of magma. *Earth-Science Reviews*, *63*(3–4), 169–247. https://doi.org/10.1016/S0012-8252(03)00035-7

Dunbar, J. A., & Sawyer, D. S. (1987). Implications of continental crust extension for plate reconstruction: An example from the Gulf of Mexico. *Tectonics*, *6*(6), 739–755. https://doi.org/10.1029/tc006i006p00739

Dziewonski, A., Bloch, S., & Landisman, M. (1969). A technique for the analysis of transient seismic signals. *Bulletin of the Seismological Society of America*, *59*(1), 427–444. https://doi.org/10.1785/bssa0590010427

Ebeniro, J. O., Nakamura, Y., Sawyer, D. S., & O'Brien, W. P. (1988). Sedimentary and crustal structure of the northwestern Gulf of Mexico. *Journal of Geophysical Research*, *93*(B8), 9075–9092. https://doi.org/10.1029/JB093iB08p09075

Ebeniro, J. O., O'Brien, W. P., & Shaub, F. J. (1986). Crustal structure of the South Florida Platform, eastern Gulf of Mexico: An ocean-bottom seismograph refraction study. *Marine Geophysical Researches*, *8*(4), 363–382. https://doi.org/10.1007/bf02084019

Eddy, D. R., Avendonk, H. J. A. V., Christeson, G. L., Norton, I. O., Karner, G. D., Johnson, C., & Snedden, J. W. (2014). Deep crustal structure of the northeastern Gulf of Mexico: Implications for rift evolution and seafloor spreading. *Journal of Geophysical Research: Solid Earth*, *119*(9), 6802–6822. https://doi.org/10.1002/2014JB011311.Received

Eddy, D. R., Van Avendonk, H. J. A., Christeson, G. L., & Norton, I. O. (2018). Structure and origin of the rifted margin of the northern Gulf of Mexico. *Geosphere*, *14*(4), 1804–1817. https://doi.org/10.1130/GES01662.1

Evanzia, D., Pulliam, J., Ainsworth, R., Gurrola, H., & Pratt, K. (2014). Seismic Vp & Vs tomography of Texas & Oklahoma with a focus on the Gulf coast margin. *Earth and Planetary Science Letters*, *402*(C), 148–156. https://doi.org/10.1016/j.epsl.2013.12.027

Ewing, J., Antoine, J., & Ewing, M. (1960). Geophysical measurements in the western Caribbean Sea and in the Gulf of Mexico. *Journal of Geophysical Research*, *65*(12), 4087–4126. https://doi.org/10.1029/jz065i012p04087

Faul, U. G., & Jackson, I. (2005). The seismological signature of temperature and grain size variations in the upper mantle. *Earth and Planetary Science Letters*, *234*(1–2), 119–134. https://doi.org/10.1016/j.epsl.2005.02.008

Filina, I., Austin, J., Doré, T., Johnson, E., Lundin, E., Minguez, D., et al. (2022). Opening of the Gulf of Mexico: What we know, what questions remain, and how me might answer them. *Tectonophysics*, *822*, 229150. https://doi.org/10.1016/j.tecto.2021.229150

Filina, I., & Hartford, L. (2021). Subsurface structures along western Yucatan from integrated geophysical analysis. *Marine and Petroleum Geology*, *127*, 104964. https://doi.org/10.1016/j.marpetgeo.2021.104964

Fischer, K. M., Ford, H. A., Abt, D. L., & Rychert, C. A. (2010). The lithosphere-asthenosphere boundary. *Annual Review of Earth and Planetary Sciences*, *38*(1), 551–575. https://doi.org/10.1146/annurev-earth-040809-152438

Gaherty, J. B., Kato, M., & Jordan, T. H. (1999). Seismological structure of the upper mantle: A regional comparison of seismic layering. *Physics of the Earth and Planetary Interiors*, *110*(1–2), 21–41. https://doi.org/10.1016/S0031-9201(98)00132-0

Gaite, B., Iglesias, A., Villasenor, A., Herraiz, M., & Pacheco, J. F. (2012). Crustal structure of Mexico and surrounding regions from seismic ambient noise tomography. *Geophysical Journal International*, *188*(3), 1413–1424. https://doi.org/10.1111/j.1365-246X.2011.05339.x

Gaite, B., Villaseñor, A., Iglesias, A., Herraiz, M., & Jiménez-Munt, I. (2015). A 3-D shear velocity model of the southern North American and Caribbean plates from ambient noise and earthquake tomography. *Solid Earth*, *6*(1), 271–284. https://doi.org/10.5194/se-6-271-2015

García-Reyes, A., & Dyment, J. (2022). Structure, age, and tectonic evolution of the Gulf of Mexico. *Earth and Planetary Science Letters*, *577*, 117259. https://doi.org/10.1016/j.epsl.2021.117259

Griffin, W. L., O'Reilly, S. Y., Afonso, J. C., & Begg, G. C. (2009). The composition and evolution of lithospheric mantle: A re-evaluation and its tectonic implications. *Journal of Petrology*, *50*(7), 1185–1204. https://doi.org/10.1093/petrology/egn033

Gueydan, F., Morency, C., & Brun, J. P. (2008). Continental rifting as a function of lithosphere mantle strength. *Tectonophysics*, *460*(1–4), 83–93. https://doi.org/10.1016/j.tecto.2008.08.012

Gurnis, M., Yang, T., Cannon, J., Turner, M., Williams, S., Flament, N., & Müller, R. D. (2018). Global tectonic reconstructions with continuously deforming and evolving rigid plates. *Computers & Geosciences*, *116*, 32–41. https://doi.org/10.1016/j.cageo.2018.04.007

Hall, D. J., Cavanaugh, T. D., Watkins, J. S., & Mcmillen, K. J. (1982). The rotational origin of the Gulf of Mexico based on regional gravity data. In J. S. Watkins & C. L. Drake (Eds.), *Studies in continental margin geology*, (pp. 115–125). AAPG. https://doi.org/10.1306/M34430C6

Hall, S. A., & Najmuddin, I. J. (1994). Constraints on the tectonic development of the eastern Gulf of Mexico provided by magnetic anomaly data. *Journal of Geophysical Research*, *99*(B4), 7161–7175. https://doi.org/10.1029/93jb02570

Hopper, J. R., & Buck, W. R. (1993). The initiation of rifting at constant tectonic force: Role of diffusion creep. *Journal of Geophysical Research*, *98*(B9), 16213–16221. https://doi.org/10.1029/93jb01725

Hudec, M. R., Norton, I. O., Jackson, M. P. a., & Peel, F. J. (2013). Jurassic evolution of the Gulf of Mexico salt basin. *AAPG Bulletin*, *97*(10), 1683–1710. https://doi.org/10.1306/04011312073

Huismans, R. S., & Beaumont, C. (2007). Roles of lithospheric strain softening and heterogeneity in determining the geometry of rifts and continental margins. *Geological Society Special Publication*, *282*, 111–138. https://doi.org/10.1144/SP282.6

Ibrahim, A.-B. K., & Uchupi, E. (1982). Continental oceanic crustal transition in the Gulf Coast geosyncline. In J. S. Watkins & C. L. Drake (Eds.), *Studies in continental margin geology* (pp. 155–165). AAPG.

Ibrahim, A. K., Latham, J. C. G., & Buffler, R. T. (1981). Crustal structure in Gulf of Mexico from OBS refraction and multichannel reflection data. *AAPG Bulletin*, *65*(7), 1207–1229. https://doi.org/10.1306/03B5948B-16D1-11D7-8645000102C1865D

IRIS Transportable Array. (2003). *USArray transportable Array*. International Federation of Digital Seismograph Networks. https://doi.org/10.7914/SN/TA1

Izquierdo-Llavall, E., Ringenbach, J. C., Sapin, F., Rives, T., & Callot, J. P. (2022). Crustal structure and lateral variations in the Gulf of Mexico conjugate margins: From rifting to break-up. *Marine and Petroleum Geology*, *136*, 105484. https://doi.org/10.1016/j.marpetgeo.2021.105484

Jackson, I., Fitz Gerald, J. D., Faul, U. H., & Tan, B. H. (2002). Grain-size-sensitive seismic wave attenuation in polycrystalline olivine. *Journal of Geophysical Research*, *107*(B12), ECV 5-1–ECV 5-16. https://doi.org/10.1029/2001jb001225

Karato, S. I., & Wu, P. (1993). Rheology of the upper mantle: A synthesis. *Science*, *260*(5109), 771–778. https://doi.org/10.1126/science.260.5109.771

Kawakatsu, H., Kumar, P., Takei, Y., Shinohara, M., Kanazawa, T., Araki, E., & Suyehiro, K. (2009). Seismic evidence for sharp lithosphere-asthenosphere boundaries of oceanic plates. *Science*, *324*(5926), 499–502. https://doi.org/10.1126/science.1169499

Kelemen, P. B., & Dick, H. J. B. (1995). Focused melt flow and localized deformation in the upper mantle: Juxtaposition of replacive dunite and ductile shear zones in the Josephine peridotite, SW Oregon. *Journal of Geophysical Research*, *100*(B1), 423–438. https://doi.org/10.1029/94JB02063

Keller, G. R., & Hatcher, R. D. (1999). Some comparisons of the structure and evolution of the southern Appalachian-Ouachita orogen and portions of the Trans-European Suture Zone region. *Tectonophysics*, *314*(1–3), 43–68. https://doi.org/10.1016/S0040-1951(99)00236-X

Keller, G. R., & Shurbet, D. H. (1975). Crustal structure of the Texas Gulf coastal plain. *The Geological Society of America Bulletin*, *86*(6), 807–810. https://doi.org/10.1130/0016-7606(1975)86<807:csottg>2.0.co;2

Klitgord, K. D., Popenoe, P., & Schouten, H. (1984). Florida: A Jurassic transform boundary. *Journal of Geophysical Research*, *89*(B9), 7753–7772. https://doi.org/10.1029/JB089iB09p07753

Kneller, E. A., & Johnson, C. A. (2011). Plate kinematics of the Gulf of Mexico based on integrated observations from the Central and South Atlantic. *Gulf Coast Association of Geological Societies Transactions*, *61*, 283–299.

Kogan, L., Fisseha, S., Bendick, R., Reilinger, R., McClusky, S., King, R., & Solomon, T. (2012). Lithospheric strength and strain localization in continental extension from observations of the East African Rift. *Journal of Geophysical Research*, *117*(3), 1–16. https://doi.org/10.1029/2011JB008516

Korenaga, J., Kelemen, P. B., & Holbrook, W. S. (2002). Methods for resolving the origin of large igneous provinces from crustal seismology. *Journal of Geophysical Research*, *107*(B9), ECV 1-1–ECV 1-27. https://doi.org/10.1029/2001jb001030

Krauss, Z., & Menke, W. (2020). The Northern Gulf Anomaly: *P*- and *S*-wave travel time delays illuminate a strong thermal feature beneath the Northern Gulf of Mexico. *Earth and Planetary Science Letters*, *534*, 116102. https://doi.org/10.1016/j.epsl.2020.116102

Ladd, W., Richard, T. B., Watkins, J. S., Worzel, J. L., & Carranza, A. (1976). Deep seismic reflection results from the Gulf of Mexico. *Geology*, *4*(6), 365–368. https://doi.org/10.1130/0091-7613(1976)4<365:dsrrft>2.0.co;2

Laske, G., & Masters, G. (1997). A global digital map of sediment thickness. *Eos, Transactions, American Geophysical Union*, *78*, F483.

Levshin, A. L., & Ritzwoller, M. H. (2001). Automated detection, extraction, and measurement of regional surface waves. *Pure and Applied Geophysics*, *158*(8), 1531–1545. https://doi.org/10.1007/978-3-0348-8264-4_11

Li, G., Chen, H., Niu, F., Guo, Z., Yang, Y., & Xie, J. (2016). Measurement of Rayleigh wave ellipticity and its application to the joint inversion of high-resolution *S* wave velocity structure beneath northeast China. *Journal of Geophysical Research: Solid Earth*, *121*(2), 864–880. https://doi.org/10.1002/2015JB012459

Lin, F. C., Moschetti, M. P., & Ritzwoller, M. H. (2008). Surface wave tomography of the western United States from ambient seismic noise: Rayleigh and Love wave phase velocity maps. *Geophysical Journal International*, *173*(1), 281–298. https://doi.org/10.1111/j.1365-246X.2008.03720.x

Lin, F. C., Ritzwoller, M. H., & Shapiro, N. M. (2006). Is ambient noise tomography across ocean basins possible? *Geophysical Research Letters*, *33*(14), 1–5. https://doi.org/10.1029/2006GL026610

Liu, W., Kung, J., & Li, B. (2005). Elasticity of San Carlos olivine to 8 GPa and 1073 K. *Geophysical Research Letters*, *32*(16), L16301. https://doi.org/10.1029/2005gl023453

Lobkis, O. I., & Weaver, R. L. (2001). On the emergence of the Green's function in the correlations of a diffuse field. *Journal of the Acoustical Society of America*, *110*(6), 3011–3017. https://doi.org/10.1121/1.1417528

Marton, G. R. G. Y., & Buffler, R. T. (1994). Jurassic reconstruction of the Gulf of Mexico basin. *International Geology Review*, *36*(6), 545–586. https://doi.org/10.1080/00206819409465475

MASE. (2007). Meso America subduction experiment [Dataset]. Caltech. https://doi.org/10.7909/C3RN35SP

Miao, W., Niu, F., Li, G., & Levander, A. (2022). Sedimentary and crustal structure of the US Gulf Coast revealed by Rayleigh wave and teleseismic P coda data with implications for continent rifting. *Earth and Planetary Science Letters*, *577*, 117257. https://doi.org/10.1016/j.epsl.2021.117257

Mickus, K., Stern, R. J., Keller, G. R., & Anthony, E. Y. (2009). Potential field evidence for a volcanic rifted margin along the Texas Gulf Coast. *Geology*, *37*(5), 387–390. https://doi.org/10.1130/g25465a.1

Minguez, D., Gerald Hensel, E., & Johnson, E. A. E. (2020). A fresh look at Gulf of Mexico tectonics: Testing rotations and breakup mechanisms from the perspective of seismically constrained potential-fields modeling and plate kinematics. *Interpretation*, *8*(4), SS31–SS45. https://doi.org/10.1190/INT-2019-0256.1

Müller, R. D., Cannon, J., Qin, X., Watson, R. J., Gurnis, M., Williams, S., et al. (2018). GPlates: Building a virtual Earth through deep time. *Geochemistry, Geophysics, Geosystems*, *19*(7), 2243–2261. https://doi.org/10.1029/2018GC007584

Müntener, O., Manatschal, G., Desmurs, L., & Pettke, T. (2009). Plagioclase peridotites in ocean-continent transitions: Refertilized mantle domains generated by melt stagnation in the shallow mantle lithosphere. *Journal of Petrology*, *51*(1–2), 255–294. https://doi.org/10.1093/petrology/egp087

Nakamura, Y., Sawyer, D. S., & Shaub, F. J. (1988). Deep crustal structure of the northwestern Gulf of Mexico. *Transactions*, *38*, 207–215. Retrieved from http://archives.datapages.com/data/gcags/data/038/038001/0207.htm

National Centre for Seismological Research (CENAIS Cuba). (1998). Servicio Sismologico Nacional de Cuba [Dataset]. International Federation of Digital Seismograph Networks. https://doi.org/10.7914/SN/CW

Nettles, M., & Dziewoński, A. M. (2008). Radially anisotropic shear velocity structure of the upper mantle globally and beneath North America. *Journal of Geophysical Research*, *113*(2), 1–27. https://doi.org/10.1029/2006JB004819

Nguyen, L. C., Levander, A., Niu, F., Morgan, J., & Li, G. (2022). Seismic evidence for lithospheric boudinage and its implications for continental rifting. *Geology*, *50*(9), 986–990. https://doi.org/10.1130/GEOL.S.19633149

Nguyen, L. C., & Mann, P. (2016). Gravity and magnetic constraints on the Jurassic opening of the oceanic Gulf of Mexico and the location and tectonic history of the Western Main transform fault along the eastern continental margin of Mexico. *Interpretation*, *4*(1), SC23–Sc33. https://doi.org/10.1190/int-2015-0110.1

Nguyen, L. C., & Mann, P. (2017). *Full-fit reconstruction of the Gulf of Mexico continental margin*. AGU Fall Meeting.

O'Reilly, S. Y., & Griffin, W. L. (2013). Mantle metasomatism. In D. E. Harlov & H. Austrheim (Eds.), *Metasomatism and the chemical transformation of rock-the role of fluids in terrestrial and extraterrestrial processes* (pp. 471–533). Springer-Verlag.

Palomeras, I., Villasenor, A., Thurner, S., Levander, A., Gallart, J., & Harnafi, M. (2017). Lithospheric structure of Iberia and Morocco using finite-frequency Rayleigh wave tomography from earthquakes and seismic ambient noise. *Geochemistry, Geophysics, Geosystems*, *18*(5), 1824–1840. https://doi.org/10.1002/2016GC006657.Received

Pérez-Gussinyé, M., Morgan, J. P., Reston, T. J., & Ranero, C. R. (2006). The rift to drift transition at non-volcanic margins: Insights from numerical modelling. *Earth and Planetary Science Letters*, *244*(1–2), 458–473. https://doi.org/10.1016/j.epsl.2006.01.059

Piccardo, G. B. (2008). The Jurassic Ligurian Tethys, a fossil ultraslow-spreading ocean: The mantle perspective. In M. Coltorti & M. Gregoire (Eds.), *Metasomatism in oceanic and continental lithospheric mantle (special Pu* (pp. 11–33). Geological Society.

Pindell, J., & Dewey, J. F. (1982). Permo-Triassic reconstruction of western Pangea and the evolution of the Gulf of Mexico/Caribbean region. *Tectonics*, *1*(2), 179–211. https://doi.org/10.1029/tc001i002p00179

Pindell, J., Miranda, E. C., Cerón, A., & Hernandez, L. (2016). Aeromagnetic map constrains Jurassic–Early cretaceous synrift, break up, and rotational seafloor spreading history in the Gulf of Mexico. In C. M. Lowery, J. W. Snedden, & N. C. Rosen (Eds.), *Mesozoic of the Gulf rim and beyond: New progress in science and exploration of the Gulf of Mexico basin* (pp. 123–153). GCSSEPM Foundation. https://doi.org/10.5724/gcs.15.35.0123

Pindell, J., Villagómez, D., Molina-Garza, R., Graham, R., & Weber, B. (2021). A revised synthesis of the rift and drift history of the Gulf of Mexico and surrounding regions in the light of improved age dating of the Middle Jurassic salt. *Geological Society Special Publication*, *504*(1), 29–76. https://doi.org/10.1144/SP504-2020-43

Pindell, J. L. (1985). Alleghenian reconstruction and subsequent evolution of the Gulf of Mexico, Bahamas, and Proto-Caribbean. *Tectonics*, *4*(1), 1–39. https://doi.org/10.1029/tc004i001p00001

Priestley, K., & McKenzie, D. (2006). The thermal structure of the lithosphere from shear wave velocities. *Earth and Planetary Science Letters*, *244*(1–2), 285–301. https://doi.org/10.1016/j.epsl.2006.01.008

Rosenthal, D. B., & Buffler, R. T. (1990). Depth to basement Gulf of Mexico region.

Sandwell, D. T., Müller, R. D., Smith, W. H. F., Garcia, E., & Francis, R. (2014). New global marine gravity model from CryoSat-2 and Jason-1 reveals buried tectonic structure. *Science*, *346*(6205), 65–67. https://doi.org/10.1126/science.1258213

Sawyer, D. S., Buffler, R. T., & Pilger, R. H. J. (1991). The crust under the Gulf of Mexico Basin. In A. Salvador (Ed.), *The Gulf of Mexico basin*, (pp. 53–72). Geological Society of America, The Geology of North America.

Schmerr, N. (2012). The Gutenberg discontinuity: Melt at the lithosphere-asthenosphere boundary. *Science*, *1480*(2007), 1480–1483. https://doi.org/10.1126/science.1215433

Shapiro, N. M., & Campillo, M. (2004). Emergence of broadband Rayleigh waves from correlations of the ambient seismic noise. *Geophysical Research Letters*, *31*(7), 8–11. https://doi.org/10.1029/2004GL019491

Shapiro, N. M., Campillo, M., Stehly, L., & Ritzwoller, M. H. (2005). High-resolution surface-wave tomography from ambient seismic noise. *Science*, *307*(5715), 1615–1619. https://doi.org/10.1126/science.1107895

Snieder, R. (2004). Extracting the Green's function from the correlation of coda waves: A derivation based on stationary phase. *Physical Review E*, *69*(4), 046610. https://doi.org/10.1103/PhysRevE.69.046610

Stein, C. A., & Stein, S. (1992). A model for the global variation in oceanic depth and heat flow with lithospheric age. *Nature*, *359*(6391), 123–129. https://doi.org/10.1038/359123a0

Stern, R. J., Anthony, E. Y., Ren, M., Lock, B. E., Norton, I., Kimura, J. I., et al. (2011). Southern Louisiana salt dome xenoliths: First glimpse of Jurassic (ca. 160 Ma) Gulf of Mexico crust. *Geology*, *39*(4), 315–318. https://doi.org/10.1130/G31635.1

Stern, R. J., & Dickinson, W. R. (2010). The Gulf of Mexico is a Jurassic backarc basin. *Geosphere*, *6*(6), 739–754. https://doi.org/10.1130/GES00585.1

Tesauro, M., Kaban, M. K., & Mooney, W. D. (2015). Variations of the lithospheric strength and elastic thickness in North America. *Geochemistry, Geophysics, Geosystems*, *16*(7), 2197–2220. https://doi.org/10.1002/2015gc005937

Van Avendonk, H. J. A., Christeson, G. L., Norton, I. O., & Eddy, D. R. (2015). Continental rifting and sediment infill in the northwestern Gulf of Mexico. *Geology*, *43*(7), 631–634. https://doi.org/10.1130/G36798.1

VEOX. (2010). Veracruz-Oaxaca subduction experiment [Dataset]. Caltech. https://doi.org/10.7909/C3MW2F2C

Vissers, R. L. M., Drury, M. R., Strating, E. H. H., & Van Der Wal, D. (1991). Shear zones in the upper mantle: A case study in an Alpine lherzolite massif. *Geology*, *19*(10), 990–993. https://doi.org/10.1130/0091-7613(1991)019<0990:SZITUM>2.3.CO;2

Wang, H., van Hunen, J., & Pearson, D. G. (2015). The thinning of subcontinental lithosphere: The roles of plume impact and metasomatic weakening. *Geochemistry, Geophysics, Geosystems*, *16*(4), 1156–1171. https://doi.org/10.1002/2015gc005784

Wapenaar, K., Draganov, D., Snieder, R., Campman, X., & Verdel, A. (2010). Tutorial on seismic interferometry: Part 1—basic principles and applications. *Geophysics*, *75*(5), 75A195–75A209. https://doi.org/10.1190/1.3457445

White, R. S., McKenzie, D., & O'Nions, R. K. (1992). Oceanic crustal thickness from seismic measurements and rare Earth element inversions. *Journal of Geophysical Research*, *97*(B13), 19683. https://doi.org/10.1029/92jb01749

Whittaker, J. M., Goncharov, A., Williams, S. E., Müller, R. D., & Leitchenkov, G. (2013). Global sediment thickness data set updated for the Australian-Antarctic Southern Ocean. *Geochemistry, Geophysics, Geosystems*, *14*(8), 3297–3305. https://doi.org/10.1002/ggge.20181

Wiens, D. A., Conder, J. A., & Faul, U. H. (2008). The seismic structure and dynamics of the mantle wedge. *Annual Review of Earth and Planetary Sciences*, *36*(1), 421–455. https://doi.org/10.1146/annurev.earth.33.092203.122633

Yamasaki, T. (2004). Localized rheological weakening by grain-size reduction during lithospheric extension. *Tectonophysics*, *386*(3–4), 117–145. https://doi.org/10.1016/j.tecto.2004.05.006

Yao, Y., & Li, A. (2016). Lithospheric velocity model of Texas and implications for the Ouachita orogeny and the opening of the Gulf of Mexico. *Geophysical Research Letters*, *43*(23), 12046–12053. https://doi.org/10.1002/2016GL071167

Zhu, H., Stern, R. J., & Yang, J. (2020). Seismic evidence for subduction-induced mantle flows underneath Middle America. *Nature Communications*, *11*(1), 2075. https://doi.org/10.1038/s41467-020-15492-6